CHAPTER 4 RESULTS AND DISCUSSION

Investigation of the DEMFC cycling operation effect on the DMFC performance degradation was conducted. Two main set-ups of the experiment were conducted to determine the effects of cycling operation on DMFC performance loss and the cause of DMFC degradation. For this experiment, the loss of cell performance was investigated and the reduction of maximum power density was determined. The evaluation of cell performance loss was performed on the start-run-stop (SRS) mode on methanol-O_2 system and step-cycling operation mode (SCO) on methanol-air system. The causes of DMFC performance were explored by using the *in situ* and *ex situ* techniques. By using the technique of polarization, linear sweep and cyclic volammogram (CV), frequency response analysis (FRA), and also, transmission electron microscopy (TEM), X-ray diffraction (XRD) and energy dispersive X-ray spectroscopy (EDX), the causes of cell performance degradation as fuel crossover, the loss of catalyst surface, and dissolution of Nafion® were detected. Moreover, the effect of heat-cycling was added to explore the Pt electrode degradation on catalyst surface loss.

4.1 Methanol-O_2 system

The effect of cycling operation on the methanol-O_2 system was investigated during test time. The stability tests of direct methanol fuel cells (DMFCs) were conducted under two different operational modes, start-run-stop (SRS) and long-running (LR) modes, to investigate the difference in performance decay of the cells. Frequency response analysis (FRA), cyclic voltammetry (CV), transmission electron microscopy (TEM), X-ray diffraction (XRD) and energy dispersive X-ray spectroscopy (EDX) were used to identify the causes of cell degradation. The cell performance test was compared and the fading behaviour of the cell under the SRS operation was evaluated during test time.

4.1.1 DMFC performance test under different operating mode of SRS and LR

The performance curves of the DMFC operated under LR and SRS modes are displayed in Figure 4.1. During test time, significant losses in performance were observed

in both operational modes.

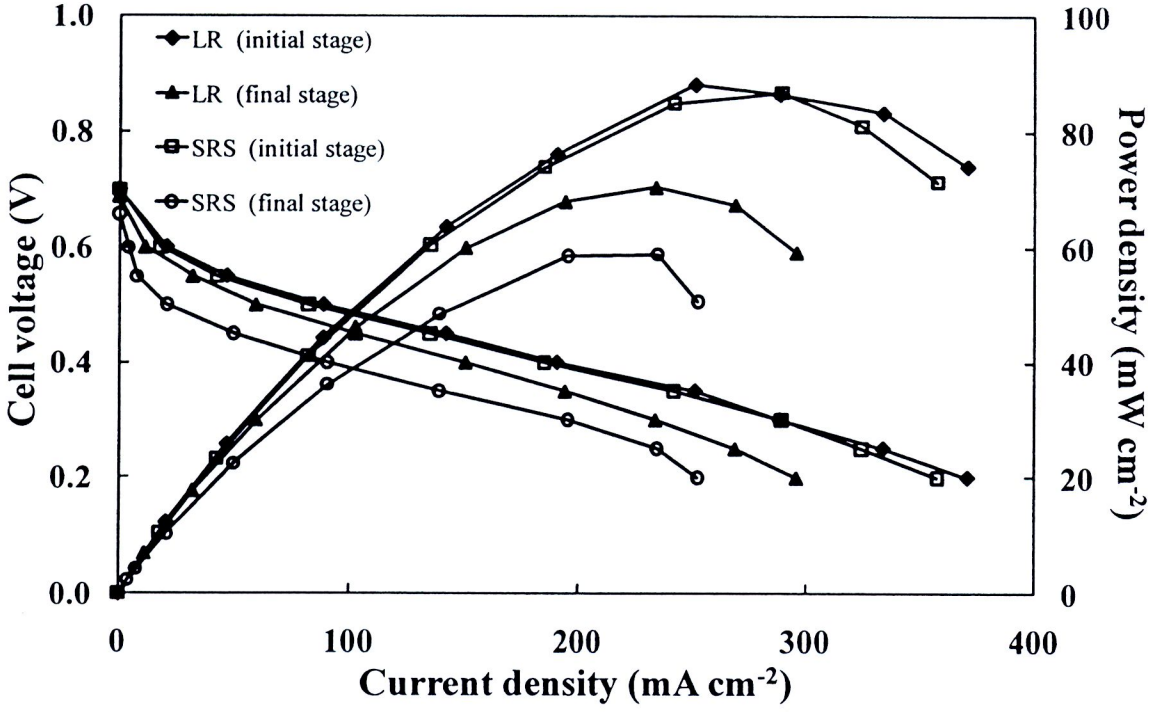

Figure 4.1 Comparison of performance of the 5 cm^2 cell active area for 5 days operation between the SRS and LR mode conditions.

The performance decays between the two operational modes were quite different. For the LR mode, the OCV did not show a significant change (0.699 V for initial and 0.687 V for final), while the OCV of the cell under SRS mode dropped from 0.701 to 0.645 V (±0.01 V). The decrease in OCV was possibly related to the methanol crossover occurring during the stopping period. At a no-load condition, the methanol concentration at the anode was relatively high, resulting in greater methanol diffusion.

In comparing the cell performance for 5 days operation with overall test time 15 h per day, the performance decay of the cell operating in the SRS mode that dropped from 86.8 to 58.8 mW cm^{-2} was higher than that in the LR mode that decreased from 88.2 to 70.3 mW cm^{-2}. The loss of maximum power density was 20% and 32% from the initial value after operating under the LR and SRS modes, respectively. Also, assume the overall test time equal to 75 h for the On-off load mode, the rate of power density degradation was 0.37 mW cm^{-2} h^{-1} and 0.23 mW cm^{-2} h^{-1} for the operation mode of SRS and LR,

respectively. Also, the rate of OCV loss was 0.16 mV h^{-1} for LR mode and 0.74 mV h^{-1} for SRS mode. This result showed that the SRS operational mode can accelerate the cell degradation process more than did the LR operational mode.

4.1.2 The causes of DMFC degradation on methanol-O_2 system

For this part, the cause of cell performance degradation of methanol-O_2 system was explored with the in-situ and ex-situ techniques. To evaluate the loss of cell performance from loss of catalyst surface, dissolution of Ru and Nafion®, and crossover of methanol and Ru were conducted in the cycling operation of the SRS mode. Moreover, the investigation of metal particle agglomeration was added to concern the occurring the increasing size of metal particle of Pt during heat-cycling condition.

In situ characterization of MEA under SRS mode

The measured impedance spectra at different life-test days during the SRS operation and its equivalent circuit model [69] are shown in Figure 4.2. The model matches the experimental data very well ($\chi^2 \cong 0.001$). This equivalent circuit represents the cell reaction at the anode and the cathode, and also the membrane resistance. For the components in this equivalent circuit, CPE2 and R4 denote the double layer capacity and the charge transfer resistance at the cathode, respectively. The constant phase element was defined by two components of CPE-T and CPE-P. The CPE was used in the model in place of a capacitor to compensate for the nonhomogeneity in the system. R2 and CPE1 describe the charge transfer resistance and the double layer capacity at the anode, respectively, while R3 and L1 designate the electro-oxidation reaction of adsorbed CO and an inductive element that induces a phase delay by the slow reaction of CO_{ads}, respectively [14]. The IR resistance or internal resistance of the membrane that was added between the anode and the cathode is denoted as R1. The variations in the equivalent circuit component values during SRS operation are summarized in Table 4.1.

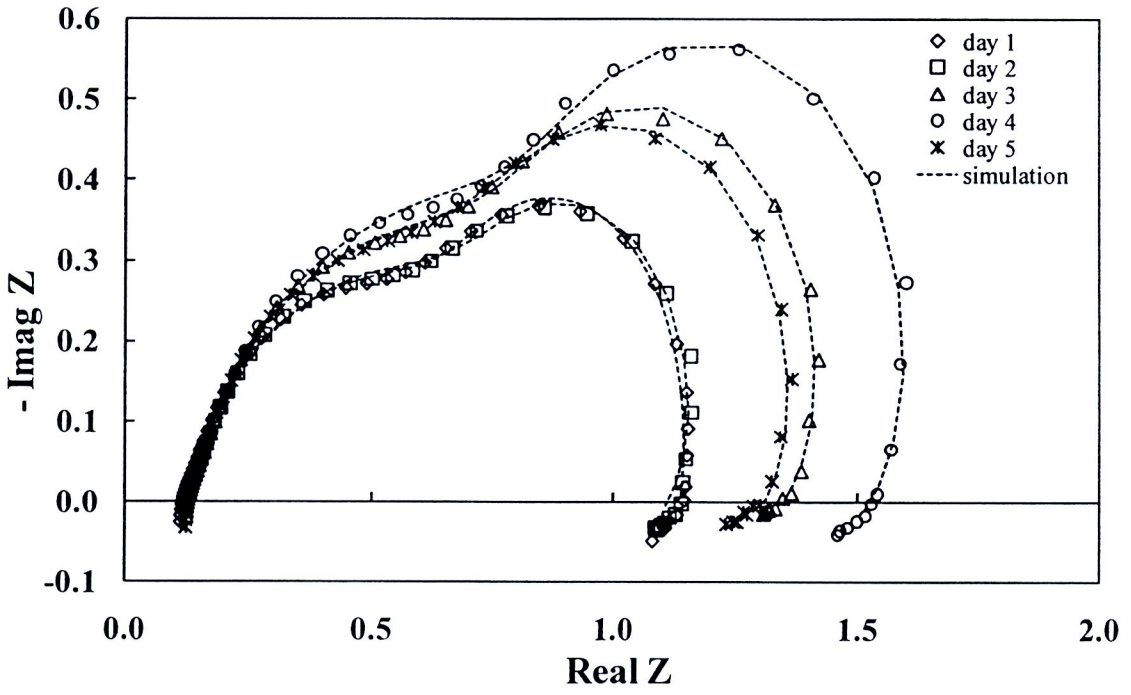

(a)

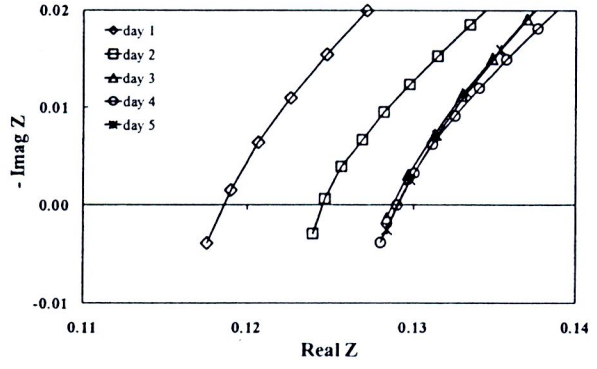

(b)

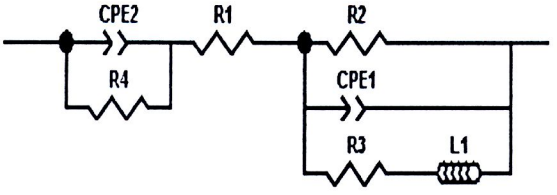

(c)

Figure 4.2 Frequency response analysis for the DMFC under SRS operation on different life-test days: (a) impedance curves, (b) impedance value at high frequency and (c) equivalent circuit model.

From the Nyquist curves, the diameter of the semicircle provides information about the magnitude of the activation resistance of the fuel cell. As displayed in Figure 4.2, the arc radius increased with time from the initial day to the fourth day of operation. This corresponded with the increase in the charge transfer resistance at both the anode (R2) and

the cathode (R4), as predicted by the equivalent circuit simulation. This means that the oxidation of methanol at the anode and the reduction of oxygen at the cathode were reduced. The anode reaction resistance (ARR) represented by (R2 x R3)/(R2 + R3) [51] was then calculated.

Table 4.1 The equivalent circuit component values during start-run-stop operation.

a) Circuit component value

Day of Measurement	Equivalent circuit component value								
	CPE2 -T	CPE2 -P	R4	R1	R2	CPE1 -T	CPE1 -P	R3	L1
Day 1 (initial)	0.06147	0.7786	0.662	0.120	0.390	0.2265	1.200	0.821	1.064
Day 2	0.06203	0.7792	0.659	0.127	0.415	0.2388	1.128	0.975	1.096
Day 3	0.06514	0.7807	0.812	0.130	0.486	0.2431	1.211	1.036	1.106
Day 4	0.06987	0.7669	0.941	0.131	0.547	0.2629	1.231	0.935	1.272
Day 5 (final)	0.06560	0.7927	0.766	0.130	0.481	0.2343	1.189	0.816	1.092

b) Anode reaction resistance and constant value

Day of Measurement	Anode reaction resistance (Ω)	Constant value (Ohm-farad)	
	(R2×R3) / (R2 + R3)	R1×CPE1-T (anode)	R1×CPE2-T (cathode)
Day 1 (initial)	0.26	0.027	0.0074
Day 2	0.29	0.030	0.0079
Day 3	0.33	0.032	0.0085
Day 4	0.35	0.034	0.0091
Day 5 (final)	0.30	0.031	0.0086

As shown in Table 4.1, the reaction resistance of the PtRu catalyst increased from 0.26 Ω cm^2 on the initial day to 0.35 Ω cm^2 on the fourth day. This is an indication of agglomeration of PtRu when the DMFC was operated at the early time. The supporting evidence for catalyst agglomeration is discussed later in the ex situ examination. However the arc radius was unexpectedly reduced on the fifth day of operation, and the cell performance was improved close to that on the third and the fourth day. In other previous works, the cell performance was recovered in the continuous-lifetest after interrupting the cell when refilling the methanol solution or oxygen gas [9,10,18]. They ascribed the performance recovery to the oxidation purge of methanol crossover from anode to cathode.

This accumulated methanol could be entirely oxidized by high over-potential of the cathode when the DMFC stopped working. It consequently resulted in the recovery of the cell performance close to the initial value when it was restarted. However, in this study, the cell recovery on the fifth day was not the same as that in the former works mentioned above. In the SRS operational mode, the cell was interrupted intermittently and was purged with N_2 gas at the cathode side before being left overnight. If the mechanism had been caused by the oxidation purge of methanol, the recovery of the cell performance would have been observed before the fifth day. Here the cell performance was not fully recovered. From the EIS data, the R_2 and R_3 on the fifth day were diminished indicating that both methanol and CO oxidation reactions were improved. This improvement should be attributed to the increase of hydrous oxide of Ru during the operation that is in favor of supporting more oxygen-containing species and yielding better methanol electro-oxidation [18].

To verify the fading behavior, the cell was tested for another day, and the polarization curve of the sixth day was compared with those of the previous days as shown in Figure 4.3. It was clear that the cell performance on the sixth day was still low but slightly better than that on the fifth day. This might be a result of catalyst cleaning effect after performing cyclic voltammogram at the end of the fifth day. Considering the ARR, it increased by 0.04 Ω cm^2 after testing in the SRS mode for 45 h (5 days). The calculated rate of anode reaction resistance (ARR) increase was 8.9×10^{-4} Ω cm^2 h^{-1}. This rate is lower than the value reported in the work of Jeon and coworkers [49]. They reported the ARR increase of 3×10^{-3} Ω cm^2 after continuously operating for 435 h which is equivalent

to the increase rate of 6.9×10^{-6} Ω cm^2 h^{-1}. Consequently from the EIS results found in this work, it could be demonstrated that the anode catalyst degradation rate under the SRS operational mode is greater than that under the non-stop operation.

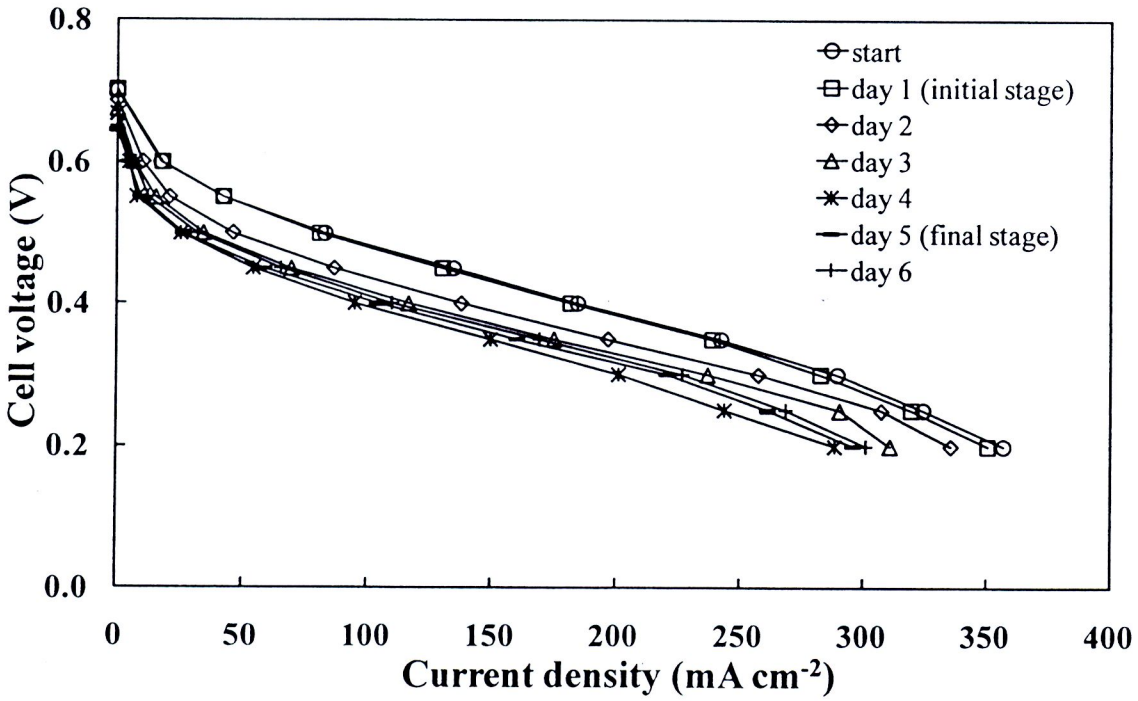

Figure 4.3 Polarization curves of the DMFC operated in SRS mode for six days.

The pure ohmic resistance can be obtained from the intersection of the arc at high frequency from the Nyquist plot. This IR resistance increased with operating time from 0.12 to 0.131 Ω cm^2. Several factors could be responsible for the increase in internal resistance. To identify the cause of this higher internal resistance, the constant values [14] of R1 x CPE-T for both the anode and the cathode were determined, as illustrated in Table 4.1. The R1 x CPE-T value increased with operating time from 0.027 (initial) to 0.031 Ω F at the anode and 0.0074 (initial) to 0.0086 Ω F at the cathode. The magnitude of the constant value at the anode (R1 x CPE1-T) was much greater than that at the cathode (R1 x CPE2-T).

Methanol stripping was performed on the initial and the final days of the SRS operation by cyclic voltammetry. The position of the methanol oxidization peak and its peak area were employed to evaluate the activity and ESA of the anode catalyst. From the methanol stripping curves on the first and the final days shown in Figure 4.4, the peak position shifted to a higher potential, from 0.39 to 0.43 V, and the peak area decreased from 0.59 to 0.56 C cm^{-2}, accounted for 5.0% reduction. The shift of the methanol oxidation peak to a higher positive potential indicated that the activity of the anode catalyst degraded [12,14].

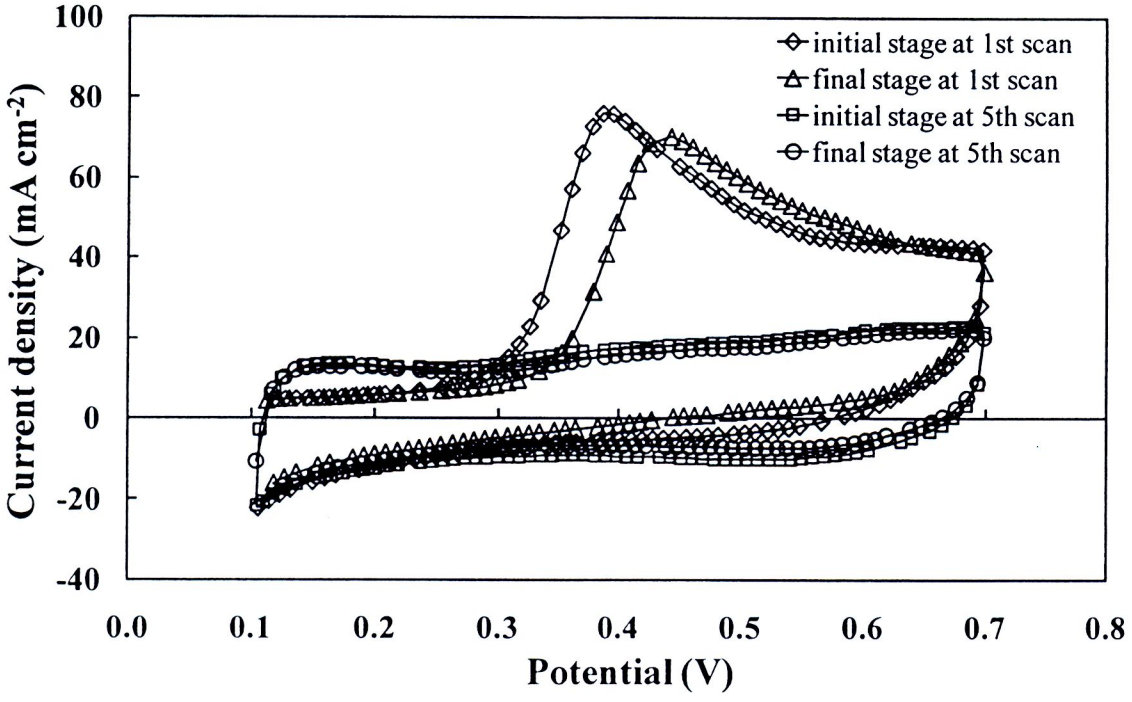

Figure 4.4 Cyclic voltammogram scan curves before and after life-testing in SRS operational mode.

Ex situ characterization of MEA under SRS mode

Figure 4.5 shows the XRD patterns of the PtRu (anode) and Pt (cathode) catalysts, respectively, before and after exposure under the LR and SRS operating modes. In case of the PtRu catalysts, the (1 1 1) diffraction plane at 2θ around 40.2° corresponded to PtRu alloy was observed in the fresh catalyst and the catalysts after life-tests in LR and SRS operational mode. For the Pt catalysts on carbon support, the major peaks at 2h of 39.8°, 46°, 67°, and 81° are corresponded to the characteristic peak of Pt. The diffraction peak at 17° and 39° can be attributed to Nafion® while the hexagonal graphite structure (0 0 2) exhibits the characteristic diffraction peak at 2θ of 26° [12]. From the XRD patterns, the average crystallite sizes of Pt and PtRu were calculated and it was found that the average PtRu crystallite size was smaller than the Pt size (3.3 nm versus 3.8 nm). The average crystallite size of Pt increased to 4.9 nm after operating both LR and SRS operational modes while that of the PtRu catalyst increased to 3.5 nm and 4.1 nm for the case of the LR and SRS operational modes, respectively. Figure 4.6 shows the TEM images of the microstructure of the anode and cathode catalysts after the life-tests. It was shown that both the PtRu and Pt catalysts had the similar tendency of agglomeration. The apparent TEM mean particle sizes of Pt catalyst increased from 5.1 to 5.5 nm, whereas the average PtRu particle size increased from 3.2 to 4.3 nm after the life-test in SRS operational mode. Here the particle sizes of the PtRu and Pt catalysts increased to 134.4% and 107.8% of their initial values, respectively.

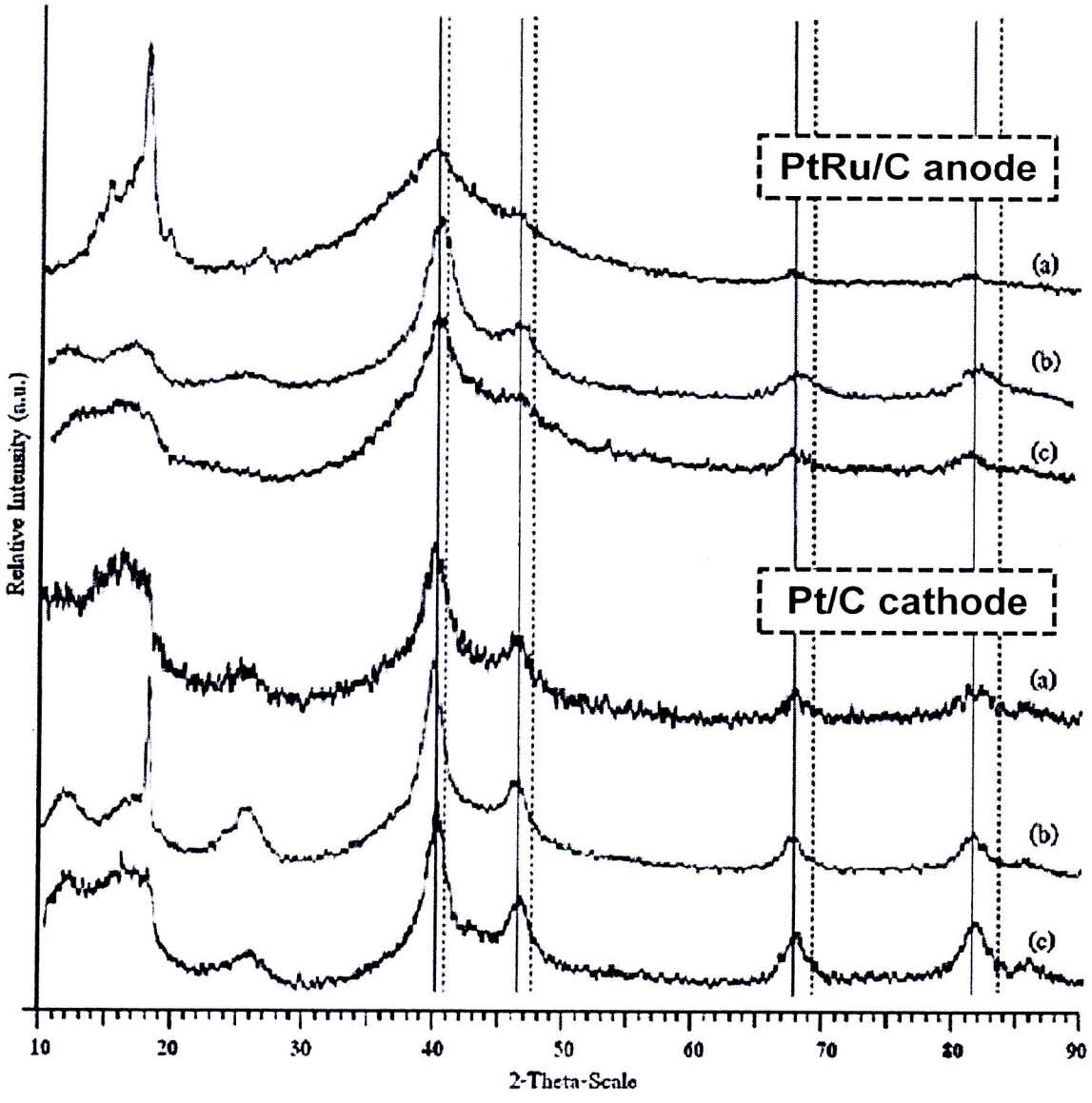

Figure 4.5 XRD patterns of the PtRu/C anode catalysts and the Pt/C cathode catalysts: (a) before testing, (b) after life-test in LR operational mode, and (c) after life-test in SRS operational mode (— represents standard peak of Pt and - - - - for Ru).

In addition, the TEM mean particle sizes of both PtRu and Pt are almost in good agreement with the crystallite sizes calculated from the XRD results, but the TEM mean particle sizes are always higher. This is similar to that was found in the work of Jeon et al. [49]. Additionally, the mean particle size of PtRu catalyst was smaller than the Pt catalyst. The small size of PtRu particles could promote migration and agglomeration of the catalyst. The enhancement of the anode catalyst agglomeration resulted from the exposure of the catalyst to a concentrated methanol solution during the stopping period in addition to the thermal cycling. From the above data, it can be seen that the anode catalyst agglomeration after operating under the SRS mode was higher than that under the LR mode. The calculated SSA of the anode catalyst after LR and SRS modes was decreased from the initial value of 86.1 $m^2 g^{-1}$ to 72.1 and 64.3 $m^2 g^{-1}$, respectively. In other words, the SSA loss of the anode catalyst increased from 16.2% to 25.3% when the operating condition for the DMFC was changed from LR to SRS mode. Nevertheless, the loss of SSA of cathode catalyst was not significantly different (49.6 and 51.0 $m^2 g^{-1}$ after LR and SRS mode, respectively, compared with the initial value of 54.7 $m^2 g^{-1}$).

Furthermore, the EDX catalyst compositions of the anode and cathode catalysts before and after the life-tests showed that the ratio of Pt to Ru (Pt:Ru) at the anode increased from 50.8:49.2 for the fresh MEA to 51.8:48.2 and 56.8:43.2 for the MEAs operated under the LR and the SRS conditions, respectively. The increase in the Pt:Ru ratio resulted from the dissolution of Ru during both operational modes, but the rate of the dissolution was accelerated by the SRS operation. The EDX results are consistent with the results of the cell polarization curve and the FRA data. The formation of formic acid, a by-product of methanol oxidation, was considered to be the main cause of the Ru-dissolution [13]. In one methanol oxidation pathway, formaldehyde and formic acid are the principal byproducts, and formic acid can further react with Ru [70]. The exposure of anode catalyst to this acid during the stop period in the SRS mode could accelerate Ru-dissolution process. Therefore, the dissolution of Ru was more severe for the SRS operation than the LR operation.

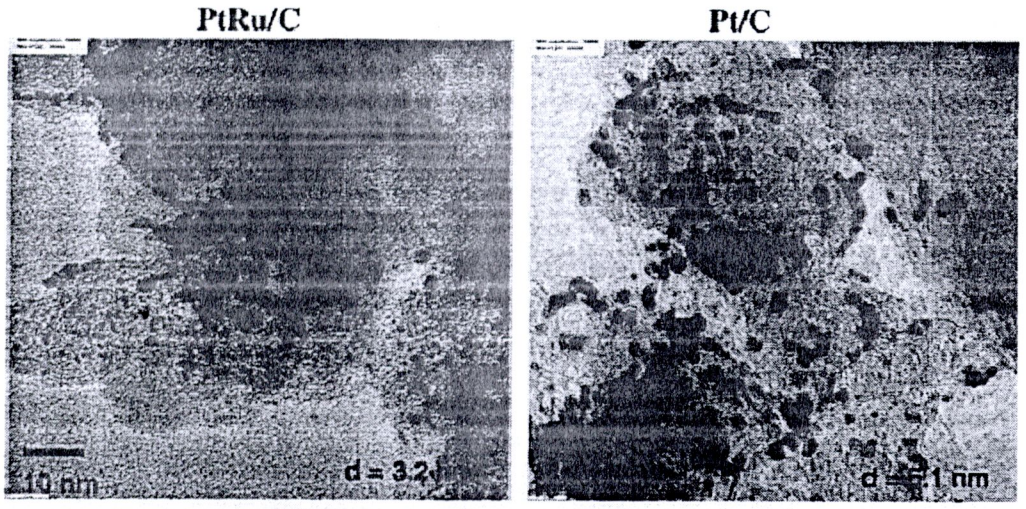

(a) Before testing

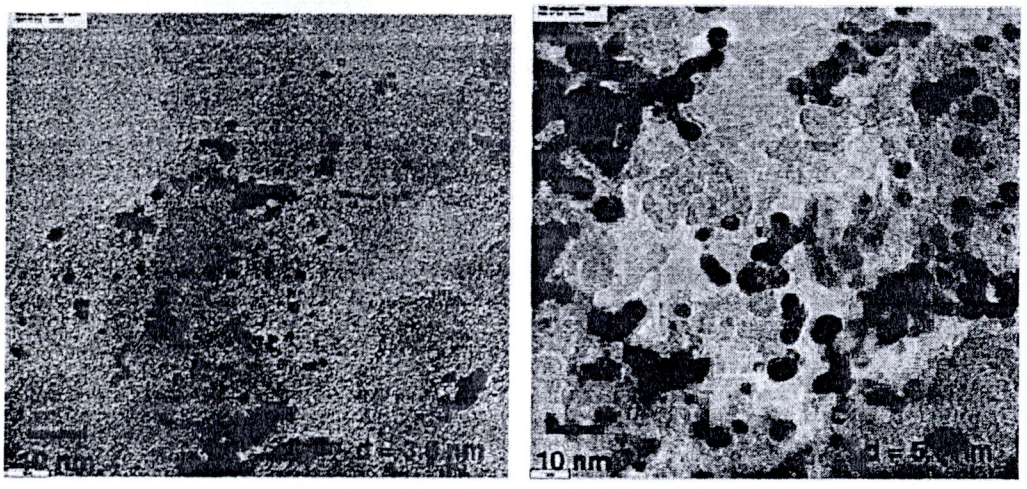

(b) After life-test in LR mode

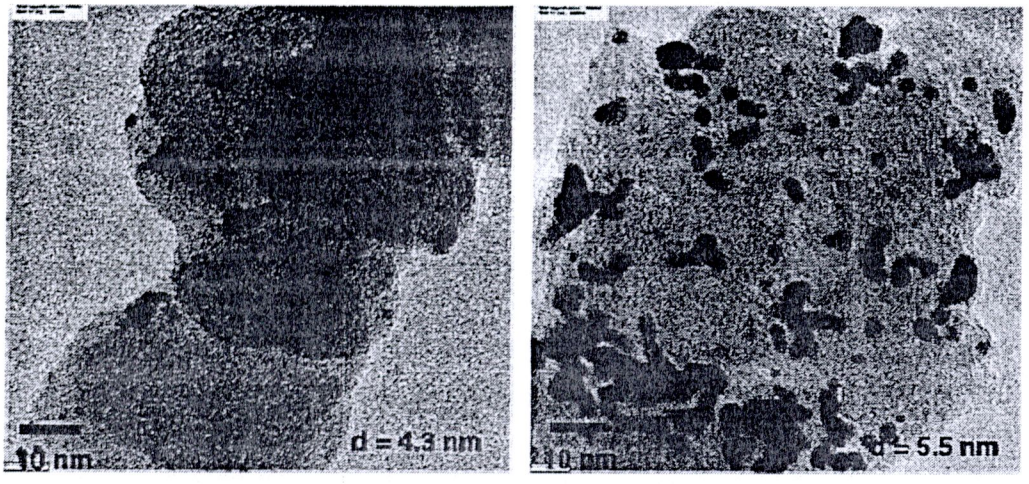

(c) After life-test in SRS mode

(TEM images)

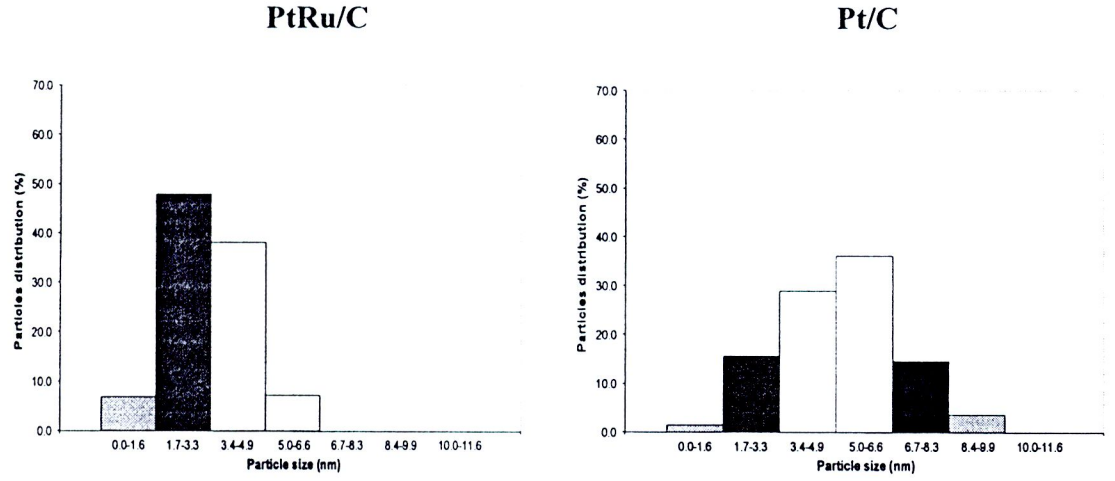

(a) Before testing

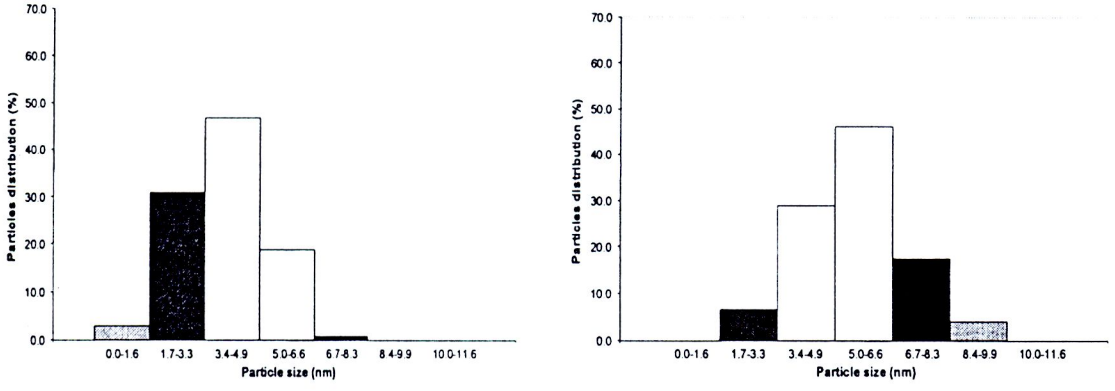

(b) After life-test in LR mode

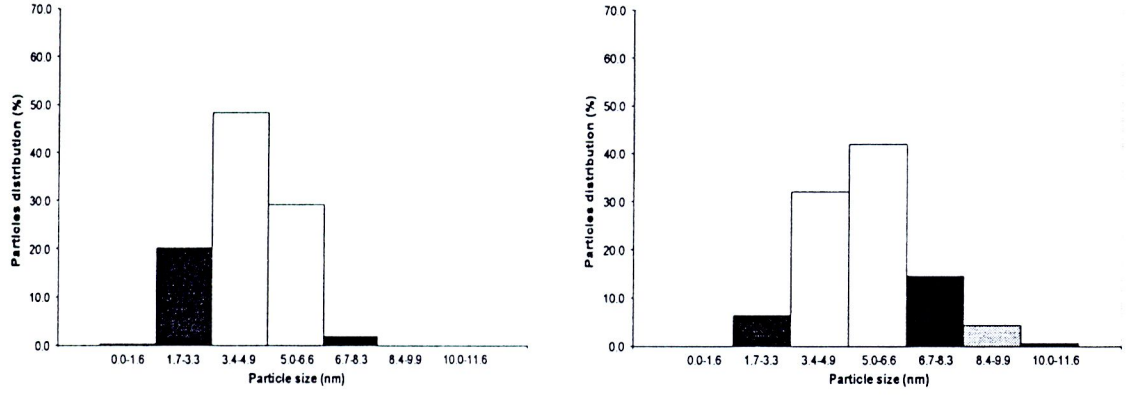

(C) After life-test in SRS mode

(Size distribution histograms)

Figure 4.6 TEM images and histograms of size distributions of the anode PtRu/C catalysts fed with methanol and cathode Pt/C catalysts fed with O_2 at 80 °C: (a) before testing, (b) after life-test in LR mode, and (c) after life-test in SRS mode.

Moreover, the EDX results of the cathode electrocatalyst confirm the Ru crossover during LR and SRS operations, since the Ru signal was also observed. The elemental composition of Ru after life-test in LR operation (Pt:Ru of 91.1:8.9) was less than that following operation in SRS mode (Pt:Ru of 84.6:15.4), indicating more severe cell degradation under the SRS condition. The crossover of Ru from the anode to the cathode by either a Ru-dissolution mechanism or the migration of metal crystallite within the catalyst layer under electrochemical stress may contribute to the activation loss of PtRu bimetallic and the reduction of methanol utilization at the anode [13,71]. The crossover of methanol due to the concentration difference can cause the swelling of membrane electrolyte and the formation of hydrous ruthenium oxide that can be dissolved in the by-product acid. Then the hydrous ruthenium oxide migrates with methanol through the membrane pore until it reaches the cathode side.

4.1.3 Effect of thermal cycling operation on agglomeration of Pt electrode

A cycle test was conducted to evaluate the effect of temperature difference and surrounding condition on the agglomeration of Pt/C electrode catalyst particles. There X-ray diffraction (XRD), and transmission electron microscopy (TEM) were employed to measure the size and size distribution of Pt catalyst particles. Moreover, the Pt/C catalyst electrodes and Nafion® 115 were prepared to membrane electrode assembly (MEA) and then demonstrated under cycle operation with liquid methanol and oxygen (O_2) at anode and cathode sides, respectively. The cell performance loss was investigated during apply methanol feed with cycling operation.

Ex situ technique characterization

The XRD patterns of the Pt/C catalyst before and after applying the cycle operation in DI water are shown in Figure 4.7. The patterns of XRD of catalyst electrode were analyzed with EVA program for peak analysis. The diffraction peak corresponding to the face-centered cubic (fcc) structure of Pt has a major peak at around 2θ of 40° (111), 46° (200), and 67° (220). Here, the Pt (220) peak was selected to calculate the mean Pt particle size because it is isolated from the diffraction peak of carbon support and Nafion® mixture

[61]. The mean particle sizes are calculated according to Scherrer's formula. The results showed that the full-width at half maximum (FWHM) was changed with different cycle periods, indicating the slight increase in Pt particle size at ~100 °C. After exposing to DI water under different cycle periods or at elevated temperature, the Pt particles became larger. It was 7.1 nm and 7.3 nm for the cycle period of 2 h and 10 h, respectively; compared to the initial particle size of 6.4 nm.

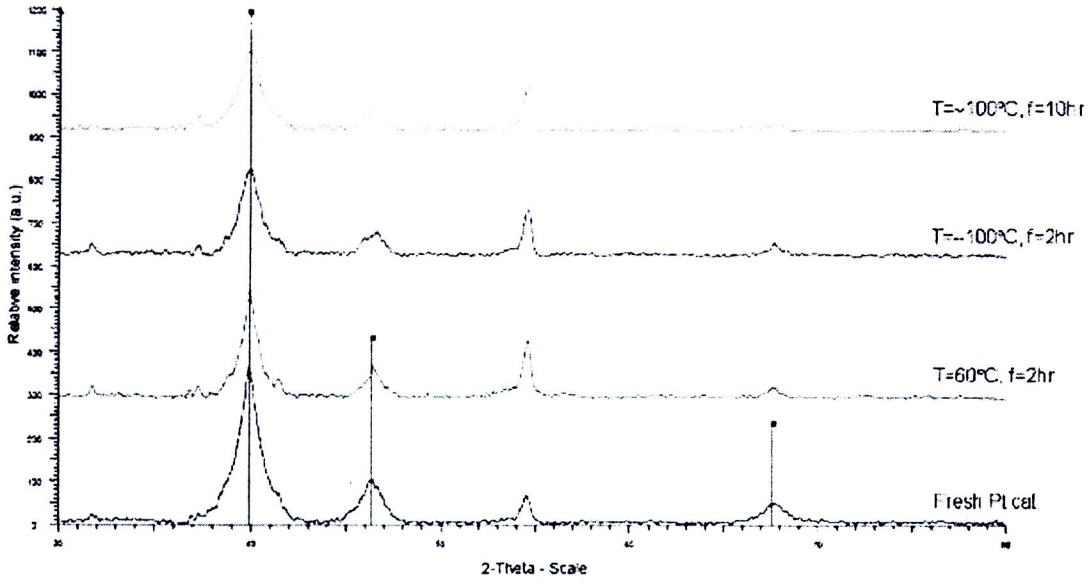

Figure 4.7 XRD patterns of Pt/C surrounded with DI water at different temperatures and cycle periods under cycle operation.

The TEM images of the Pt/C after and before cycle operation are also shown in Figure 4.8. It seems that after the cycle operation, the catalyst particles grew to some extent. The apparent mean particle size increased from initial fresh catalyst of 2.9 nm to 3.8 nm and 3.9 nm at the cycle period of 2 h and 10 h, respectively as concluded in Table 4.2. The effect of cycle period on the Pt catalyst size increase obtained from XRD was higher than that from TEM. This phenomenon may be explained by a migration of catalyst crystallites. In addition, increasing temperature from 60 °C to 100 °C at the same cycle period enhanced agglomeration of Pt particle size increasing from 3.4 to 3.8 nm, respectively. At high temperature, growing of catalyst particles came from the migration of Pt. Moreover, at high temperature, Pt particles migrated from the edge of Vulcan XC 72

carbon support to inside the carbon. Also with short cycle period, some of the metal Pt particles are detached from the carbon support as shown in Figure 4.8 (c).

Table 4.2 Particle size and specific surface area loss of the Pt/C catalysts surrounded with DI water.

Metal Pt/C		Mean particle size		Specific Surface Area	Loss of SSA
		XRD	TEM		
Cycle operation	Temperature	nm	nm	m^2/g	%
Fresh Pt catalyst (25°C)		6.4	2.9	94.7	-
f = 2 h	60°C	6.6	3.4	82.6	12.8
	~100°C	7.1	3.7	72.8	23.1
f = 10 h	~100°C	7.3	3.9	71.8	24.1

The specific surface area (SSA) of the catalyst particle was calculated from the mean particle size by the following equation, assuming all the particles are in spherical shape [12]: $S = \frac{6 \times 10^4}{d\rho}$ where d is the mean particle size in Å , and ρ is the metal density (Pt = 21.4 g cm^{-2}). So the SSA is the inverse proportion to the mean particle size of catalyst particles, and the SSA loss can be derived from the particle sizes of Pt particle before and after exposure to methanol solution under cycle operation at different temperatures. Increasing the exposed temperature from 60°C to 100°C at the same cycle period of 2 h, the SSA loss was increased from 12.8% to 23.1%, respectively.

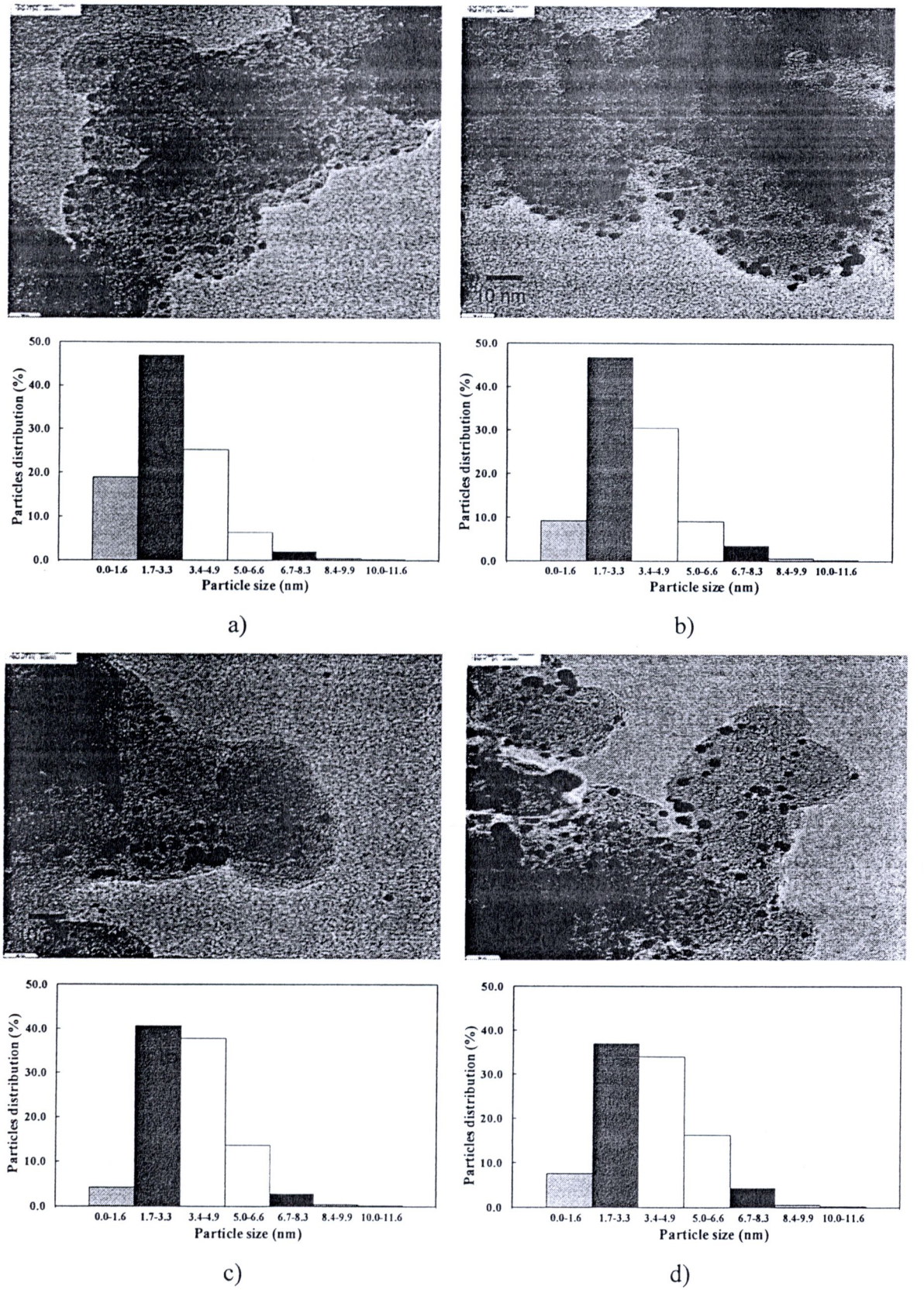

Figure 4.8 TEM images and size distributions of the Pt surrounded by DI water under cycle operation (a) fresh Pt/C, (b) f = 2 h, 60°C, (c) f = 2 h, ~100°C and (d) f = 10 h, ~100°C.

In methanol surroundings, the XRD and TEM results revealed the acceleration of Pt particle size increment under different cycle periods compared to the continuous operation as shown in Figure 4.9 and 4.10. The XRD pattern of Pt catalyst exposed to methanol solution under the continuous and cycle operation at 60 °C shows the increasing of Pt size from 6.8 nm and 7.5 nm, respectively. The temperature effect on the Pt particle size under the continuous operation showed the slight agglomeration of Pt particles from 6.4 nm to 6.6 nm when the temperature increased from 25°C to 60°C, respectively. Also, at 60°C, from the TEM images, the Pt particle size increased from 3.5 to 3.7 nm when it was exposed under the continuous and cycle operation, respectively. For the effect of temperature, again the Pt particle size was slightly increased from 3.4 to 3.5 nm with the temperature increased from 25 °C to 60 °C, under the continuous operation. The results revealed that the cycle operation can accelerate the agglomerated of Pt on carbon support than the continuous operation at the same temperature.

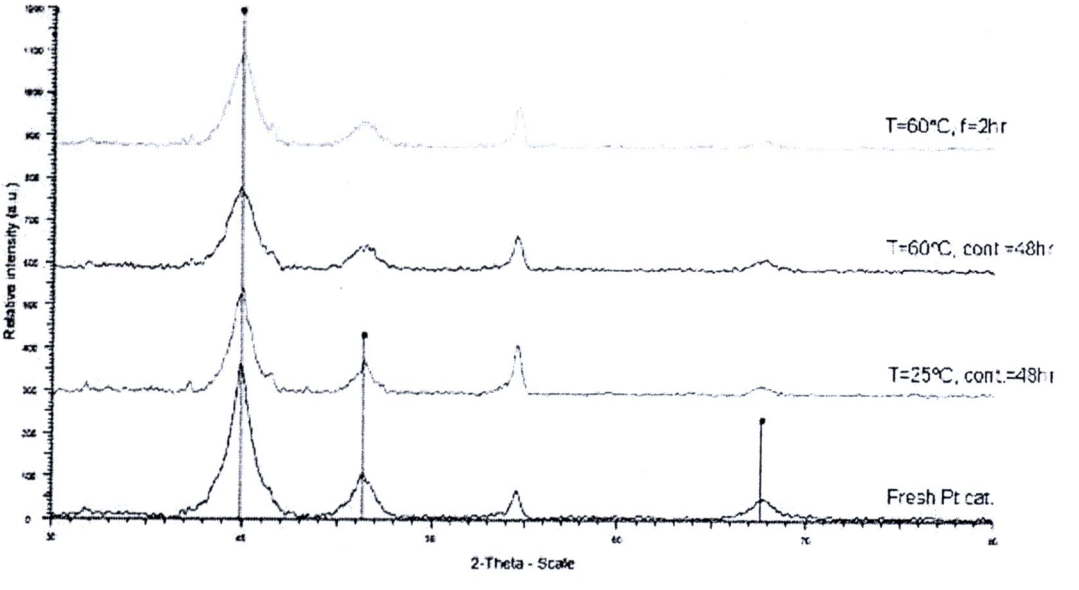

Figure 4.9 XRD patterns of Pt on C after exposure to methanol solution under cycle operation at different cycle parameters.

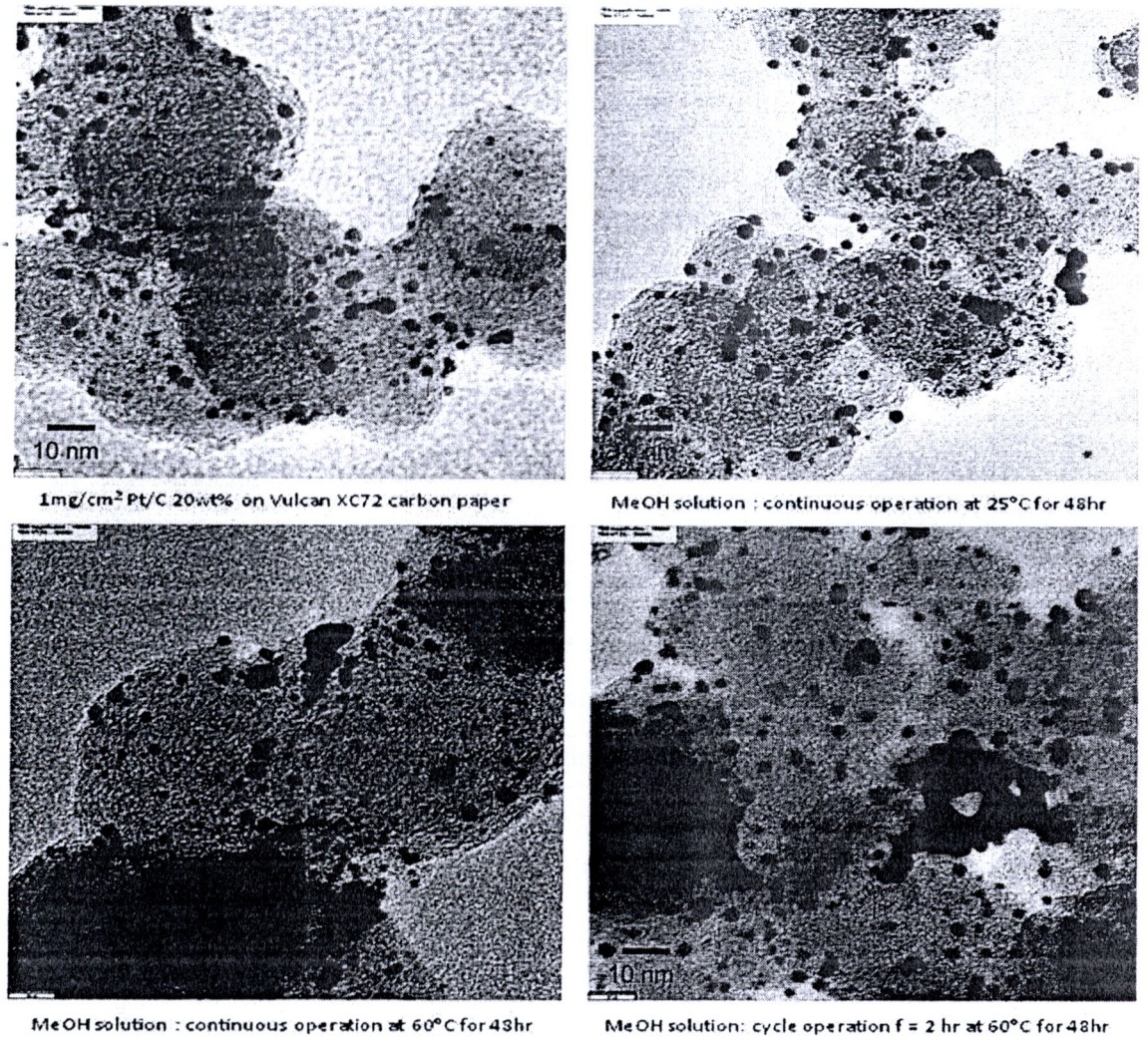

Figure 4.10 TEM images of Pt on C after exposure to methanol solution under cycle operation at different cycle parameters.

In comparing between the effect of methanol solution and DI water at the same cycle operation, the particle sizes were 3.7 nm and 3.4 nm, respectively. The higher Pt growth acceleration in methanol and DI water can be explained as follows: 1) Pt catalyst electrode surface is oxidized by methanol, then 2) the intermediate acid products on Pt surface such as formaldehyde and formic acid are formed, and 3) the cycle operation gave different chemical stresses as different acid concentrations since the amount of methanol oxidation products depend on the temperature change, resulting in migration of catalyst crystallites.

Moreover, the same electrode was assembled as a MEA and then the extra cell testing was performed. This cell testing gave results on the polarization curve of methanol and hydrogen feed and also the on the performance curve of hydrogen feed was interpreted with program STATISTICA version 6.0 to determine the activation loss (A) and the ohmic loss (r) value as shown in the next title of cell testing.

In situ technique characterization

The investigation of fuel cell performance degradation fed with methanol solution at anode and oxygen at cathode was performed during cycle operation. The cycle operation condition at 6 h cycle period and 60°C cell temperature was chosen. The cell performance is shown in Figure 4.11. During this cycle operation, the loss of cell performance was detected. The reduction of the open circuit voltage (OCV) of DMFC from 0.47 to 0.44 V exhibits that methanol fuel crossover is slightly increased from beginning (1^{st} day) to the end (4^{th} day) of cycle operation. Also, the power density of the cell was dropped by 20.1% from the application of initial cycle operation. The activation loss was caused by the catalyst agglomeration with poor active surface area [62]. Also, the CO intermediate product of methanol oxidation adsorbed on Pt surface and reduced the specific surface area of Pt [8]. This gave low oxidation of methanol at Pt surface and then provided more liquid fuel methanol crossover from the anode side to the cathode side with increasingly differing methanol concentration at Pt catalyst surface.

Another performance degradation investigation was performed on the cell with methanol feed. The fuel feed was switched from methanol to H_2 at anode side and the cell was tested at operating temperature of 60°C. The cell performance curve shown in Figure 4.12 was dropped after feed methanol into the cell at 1^{st} (initial) day and more decayed when stop in 4^{th} (final) day of cycle operation. This power curve was further interpreted for the activation loss (A) and ohmic loss (r) by using STATISTICA version 6.0 as displayed in Figure 4.13. The results showed the increasing value of A form 0.043 to 0.055 V and r from 0.366E-3 to 0.418E-3 kΩ cm^2 (compared with the reference value of A = 0.03 V and r = 0.245E-4 kΩcm^2 for PEMFC operation at 80 °C [38]). The increasing values of A and r revealed that the charge transfer was reduced due to the poor active surface from the

catalyst particle migration and agglomeration during cycle operation. Also, they might have caused the reduction of methanol oxidation on Pt catalyst surface with poisonous intermediates (CO) from the oxidation pathway on Pt surface. These can be the cause of the cell performance loss due to the catalyst agglomeration [12] and also the fuel crossover [7] during cycle operation.

This cycle operation showed the growth of Pt catalyst particle size accelerated especially in methanol solution environment through the migration of the crystal under different chemical stress with methanol oxidation during cycling operation. With liquid methanol fed on the Pt catalyst electrode at anode of the MEA, the cell performance degradation was caused by the loss of catalyst surface area due to particle agglomeration and the reduction of OCV due to fuel crossover [9].

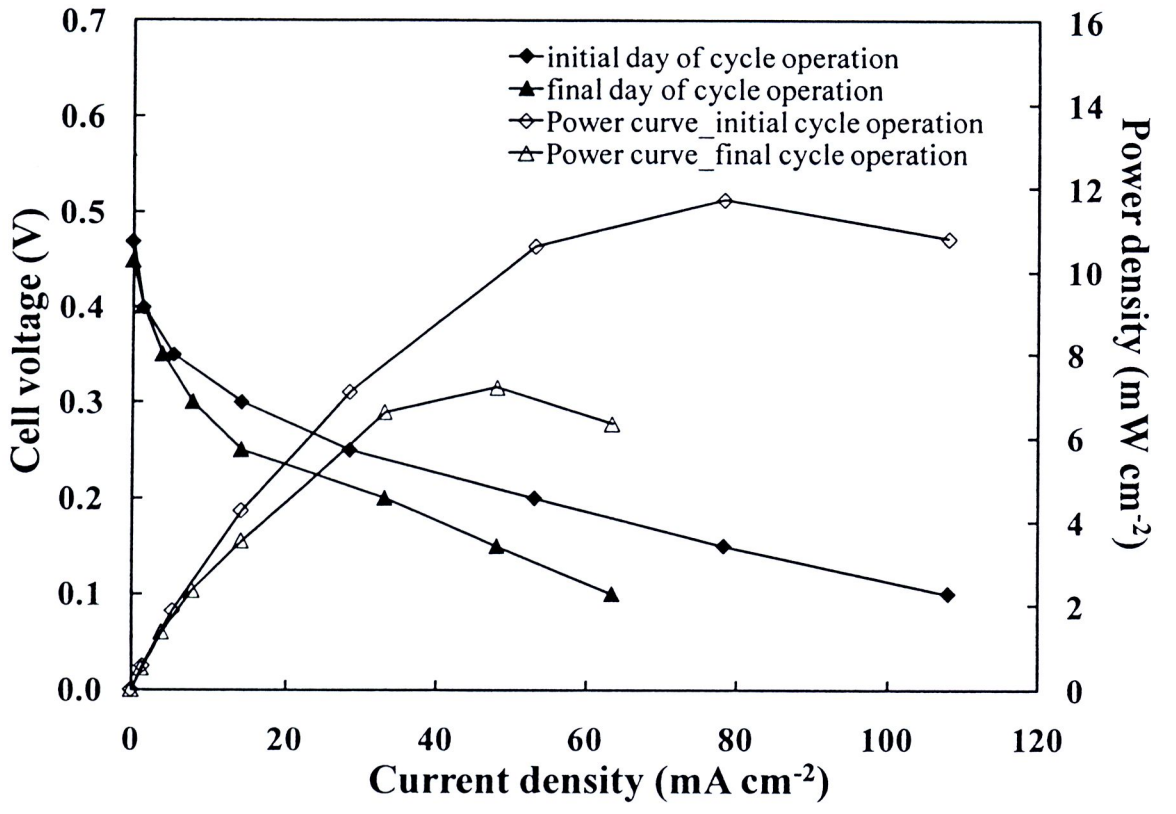

Figure 4.11 Cell performance curve at 1st (initial) day and 4th (final) day with liquid methanol and O_2 feed on Pt electrode under cycle operation at anode and cathode, respectively.

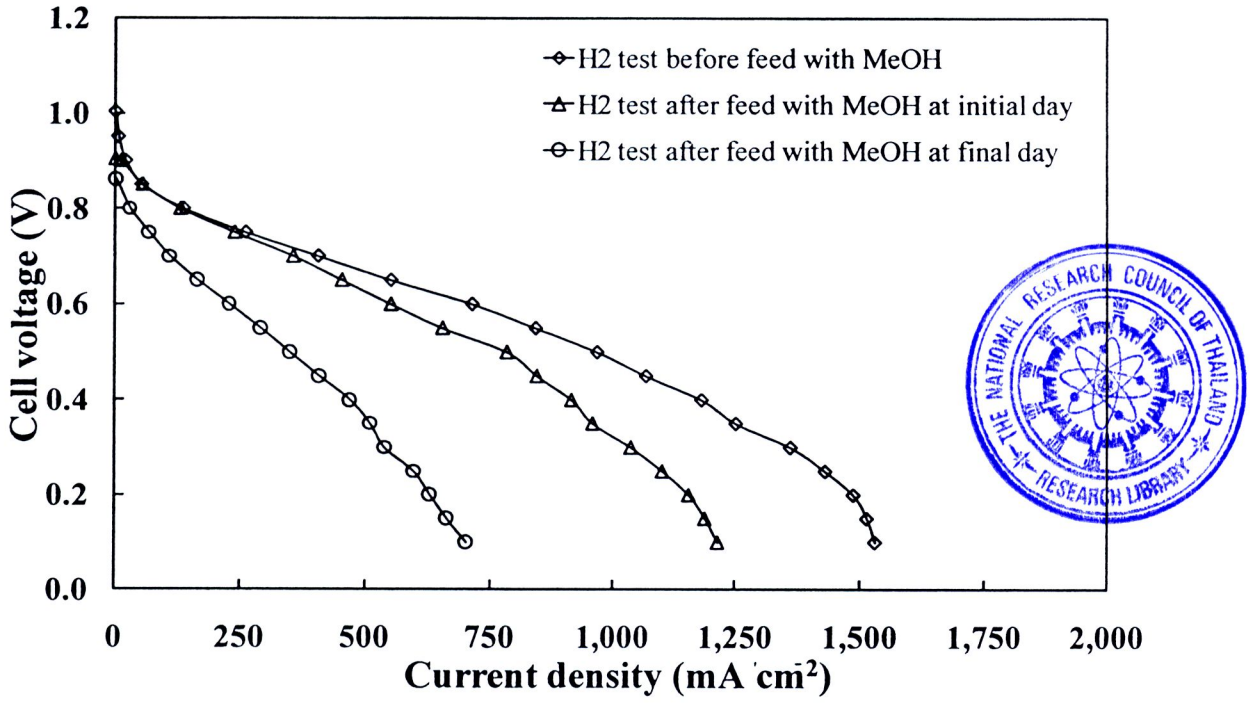

Figure 4.12 Cell performance curve at 1st (initial) day and 4th (final) day with H_2/O_2 feed on Pt electrode after cycle feed with methanol.

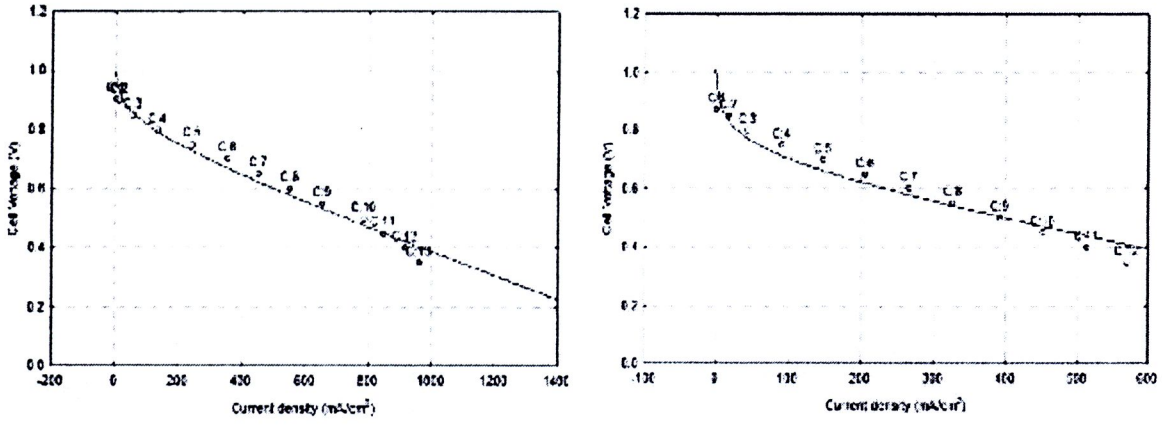

a) 1st (initial) day b) 4th (final) day

Figure 4.13 Performance curve interpretation with program STATISTICA version 6.0 to determine the activation loss (A) and the ohmic loss (r) value.

4.2 Methanol-air system

The effects o f c ycling operation on the methanol-air system were investigated during test time. The stability tests of direct methanol fuel cells (DMFCs) were conducted under two different operational modes, step-cycling operation (SCO) and long-running for 100 h (LR-100) modes, to investigate the difference in performance decay of the cells. The measuring techniques of Cell and anode polarization, Frequency response analysis (FRA) and linear sweep and cyclic voltammetry (LSV and CV) were used to identify the causes of cell performance loss and fading behaviour. The cell degradation under the SCO operation was compared with the LR-100 operation.

4.2.1 The degradation of DMFC performance operation with SCO

Single cell performances of the DMFC operated at 70 °C after different test times are shown in Figure 4.14. The polarization curves showed significant reduction in performance as test time increased. The current density at 300 mV decreased from 230 mA cm^{-2} to 90.9 mA cm^{-2} after 100 h or 10 cycles of the load profile (see Figure 3.5) It was also observed that there was a dramatic fall in performance during first 40 h. Under SCO mode, cell open circuit voltage (OCV) was reduced from 538.3 to 482.7 mV after 100 h of test time. Also, power density of the single cell decreased from 40.7 to 10.7 mW cm^{-2}.

The data of the cell performance curves indicated that during the operation of SCO, the major loss in voltage was occurred at the low current density region. First the major contribution to OCV loss may be come from the methanol crossover to the cathode and second major contribution to cell voltage loss at low current density may be come from the problem on the catalyst surface area as an agglomeration of catalyst and a dissolution of Ru; both causes being linked to a decrease in catalyst area of the anode.

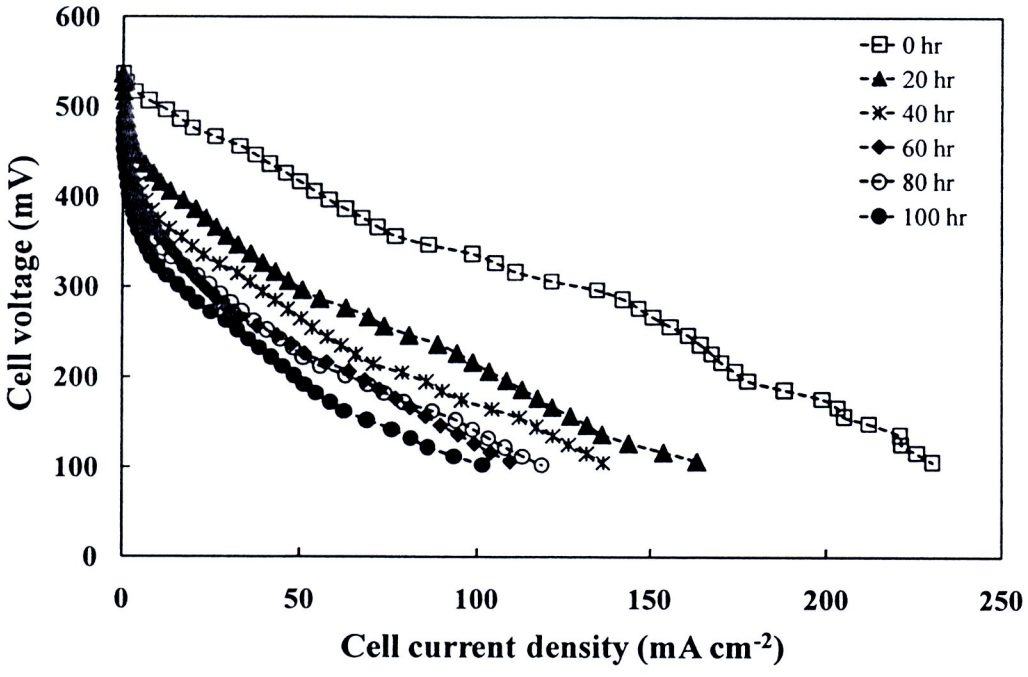

Figure 4.14 Performances of DMFC single cell during 100 h test time with SCO mode.

This cell performance loss was combined with the degradation effect of the anode and the cathode. Then, to identify the drop in cell polarization, the polarization curves of anode and cathode at initial (0 hr) and final (100 hr) time of SCO mode was measured. The results of polarization show the reduction of cell and cathode performance, and also, the increment of anode performance as displayed in Figure 4.15. Comparison on the loss of polarization, the decrease of cell performance was occurred during test time.

At the anode, the curve of anode polarization was indicated on the increase of anode potential with operation time. The anode potential at zero current density was changed by 0.45 mV to 1.07 mV under SCO mode of 100 h. Furthermore, at the current density of 10 mA cm^{-2}, the anode potential increased from 239.9 mV (initial) to 340.1 mV (final). This increment of anode potential may be associated with the decreasing in surface area of catalyst caused by catalyst agglomeration [78] and loss of unalloyed Ru [14]. Moreover, the right-shift from initial of the anode polarization curves at low current region of 0-10 mA cm^{-2} shows the instability of the catalyst surface due to the changes in electron and proton conductivity under on-off load profile operation. Such circumstances may have

caused Ru dissolution and unalloyed Ru migration to the cathode side along with methanol crossover [14, 75] which led to a major decrease in cathode performance.

At the cathode, for the drop of cathode polarization, the possible reasons that can be explain on the cathode potential reduction are (1) the influence of methanol cross over on Pt site and the competition between methanol oxidation and oxygen reduction reactions on the Pt surface at the cathode [82] and (2) the adsorption of RuO_x (from Ru crossover) on the Pt surface which can reduce the surface area for oxygen reduction [17].

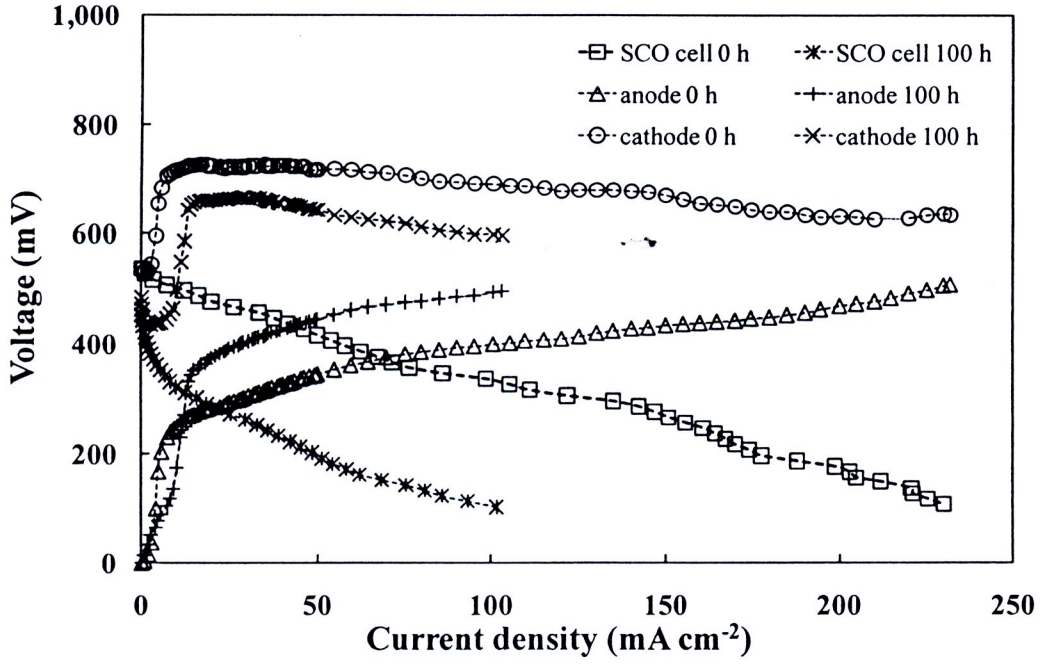

Figure 4.15 Polarization of cell operated with SCO mode, anode and cathode at 0 and 100 hr.

The dissolution of Ru in catalyst composition was indicated by the increase value of onset potential of the PtRu at the anode side. Figure 4.16(a) shows the linear sweep votammogram (LSV) curves for methanol oxidation at 70°C. Form Table 4.3, the onset potentials of the anode during 100 hr test with SCO was shifted from 289.9 (initial) to 362.8 (final) mV vs. RHE. The increased onset potential may be come from the change of catalyst composition when the ratio of ruthenium (Ru) was reduced as reported by Wang et al. [85]. Furthermore, the influence of CO_{ads} poison on catalyst surface can increase due to the loss of Ru [86].

From the linear sweep voltammogram, Tafel slopes (Figure 4.16 (b)) and values of exchange current densities were determined (Table 4.3). The value of Tafel slope increased with test time from 173.6 to 184.3 mV dec^{-1} at low potential region. The increase of the Tafel slope showed that the reaction rate of methanol oxidation was reduced. In addition, the exchange current density during the test time decreased from 0.807 to 0.387 mA cm^{-2} at the low potential region. The decrease of the exchange current density implied the loss of performance because of the Ru dissolution. These results were expected from the increasing onset potential of methanol oxidation.

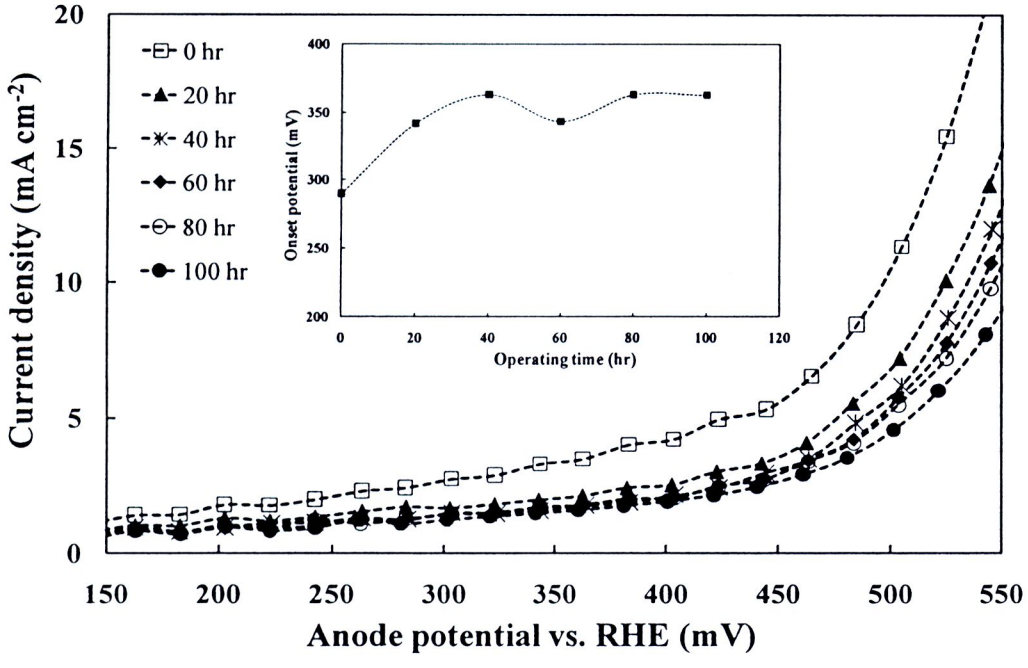

(a)

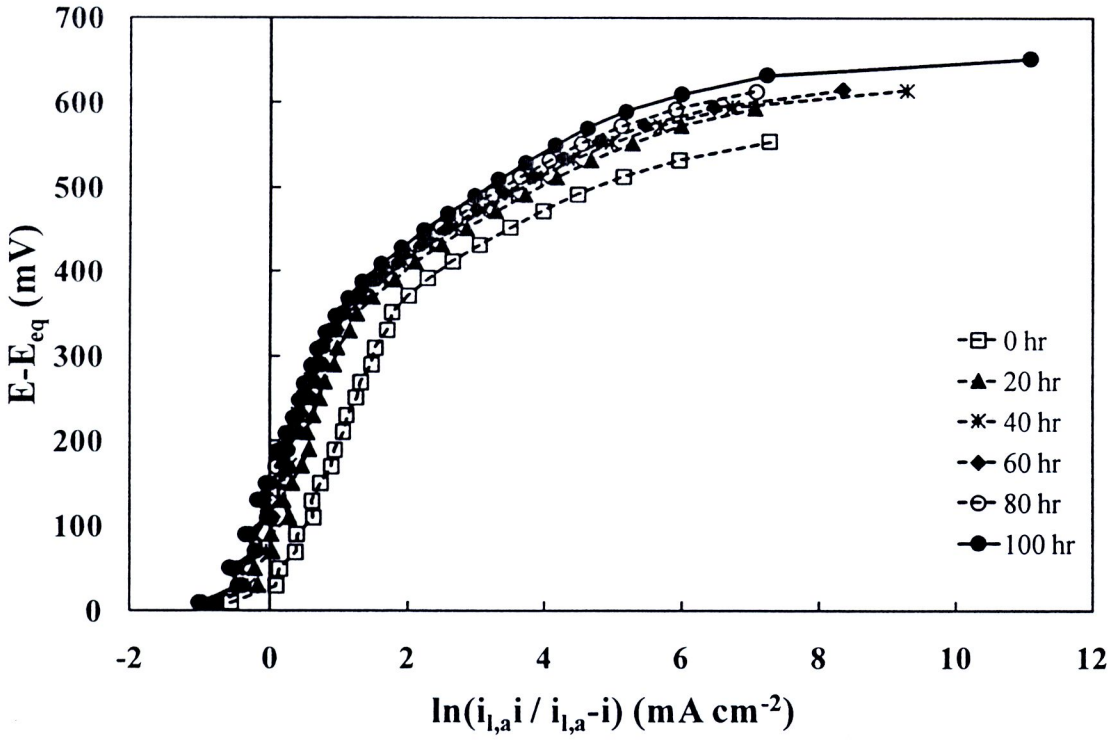

(b)

Figure 4.16 Linear sweep potential of anode Pt-Ru/C catalyst at different test times during the SCO mode: (a) onset potential and (b) Tafel plot.

Table 4.3 The value of anode onset potential, Tafel slope and exchange current density for SCO mode.

Operation time (hr)	Anode (PtRu/C)		
	Onset potential (mV vs. RHE)	Tafel slope (mV dec^{-1})	Exchange current density (mA cm^{-2})
0	239.9	173.6	0.807
20	342.0	172.3	0.468
40	363.1	183.1	0.421
60	343.4	174.7	0.393
80	363.2	181.6	0.422
100	362.8	184.3	0.387

The investigation of methanol stripping performance was done by keeping the anode at a constant potential of 0.1 V versus RHE during methanol adsorption on the surface of the Pt-Ru/C catalyst over a 20 min period. Later the un-adsorbed methanol molecules were purged by de-ionized water and a CV scan was applied in order to oxidize the adsorbed methanol molecules. The peak position of methanol oxidization could be used to evaluate the activity and electrochemical surface area of the Pt-Ru/C catalyst. Voltammograms of methanol stripping under the SCO mode as displayed in Figure 4.17 indicated that the oxidation of adsorbed methanol on PtRu started at the potential around 250 mV vs. RHE and initial time of 0 to 40 h. After that, the onset potential of methanol oxidation peaks was shifted to higher potential around 450 mV. It had been mentioned that the formation of formaldehyde and formic acid, a principal by-product of methanol oxidation, might cause the Ru-dissolution [75].

Our results indicate that the Pt-Ru/C catalyst surface lost a fraction of the unalloyed Ru which is normally believed to promote CO_2 formation on Pt surface. Such a loss of Ru has been reported to be responsible for the formation of acetic acid intermediate and CO_{ads} species as by-products of methanol oxidation. At the high current density region with respect to the load profile, the acid environment formed by accumulated intermediates could also accelerate leaching of Ru [76] as well as PtRu compositional changes [77]. Such a composition change gave a rising of the low catalyst activation at low current density and then a different pathway for methanol oxidation during the SCO mode. As a result, the complete methanol oxidation current was reduced as shown in Table 4.4 and by-product oxidation currents (as acid intermediates and CO_{ads} species) may have been promoted. However, due to the loss of Ru, the ratio of Pt was increased and this could have caused more oxidation current of CO_{ads} on Pt catalyst surface after 60 h since the oxidation current of CO and methanol on PtRu was lower than Pt, while, the starting point of CO and methanol oxidation of PtRu was occurred before Pt as reported by Láňová et al. [87].

The oxidation of methanol yields CO_2 on smooth polycrystalline platinum and starts at 550 mV vs RHE [87]. In addition, when the anode potential reaches more than 400 mV during test time, the acid environment was increased due to acetic acid formation at Pt(110), Pt(100), and polycrystalline platinum electrodes.

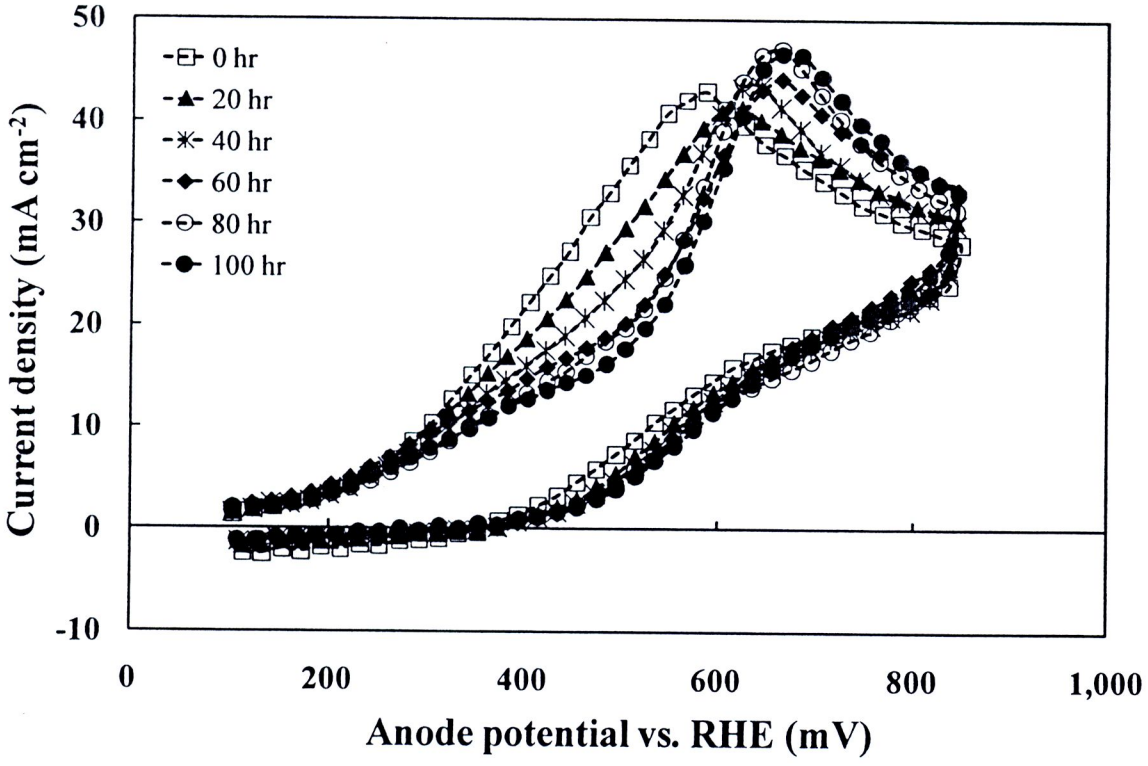

Figure 4.17 Methanol-stripping test of anode Pt-Ru/C catalyst at different test times during the SCO mode.

Table 4.4 Anode peak currents and position of methanol oxidation at different test times of the SCO mode.

Operating hour (hr)	Oxidation current at anode	
	Peak current ($mA\ cm^{-2}$)	Peak position (mV vs RHE)
0	43.0	586.9
20	39.1	603.2
40	44.0	623.9
60	44.1	664.0
80	46.7	664.5
100	46.6	684.5

However, the acetic acid formation was retarded at the potentials below 0.4 V, where acetaldehyde oxidation appeared as the dominant process [13]. This led to a

decrease in the catalyst surface area due to accumulation of poisonous intermediates or impurities. Furthermore, the oxidation peak potentials increased from 586.9 to 684.6 mV vs RHE. There has been reported a broadening of CO_{ads} oxidation peak observed at 700 mV and 800 mV (vs. RHE) for PtRu/C and Pt/C, respectively [51].

Changes in the electrochemical resistance of the anode were explored by the method of frequency response. The Nyquist plots obtained at different times of the SCO condition (Figure 6) show a distorted kinetic semicircle at higher frequencies, which is followed by a mass-transport related semicircle at the low-frequency. Similar to previous reports on DMFC anode impedance investigations [73], the data displayed different features with significant mass-transport limitations at the low frequency of 0.2-0.4 Hz. This effect may be come from a low methanol flow rate through diffusion layer to the catalyst layer due to the delaminating of backing layer from membrane and the denseness of textile and carbon contained at diffusion layer. In addition, at the very low frequency of 0.1-0.2 Hz, the inductive behavior element was detected up to test times of 40 hr because the slowness in relaxation of CO_{ads} coverage has been identified previously at the very low frequency range [14]. However, after that, the dominant of inductive behavior was reduced because of the more occurring of Ru dissolution.

Moreover, the decrease of the internal resistance value of 0.379 to 0.253 Ω cm^2 at high frequency was detected by using FRA. The internal resistance values may have been reduced due to the swelling of the membrane. The possible reason for a reduction of internal resistance which was implied as a good ion conductor of polymer was due to the presence of fixed charge sites and the presence of free volume called "open space". Since, in fact, Nafion® can accommodate so much water that its volume increases up to 22% when fully hydrated, however, for strongly polar liquid, such as alcohols, it can cause Nafion® to swell up to 88% [88]. Swelling of membrane was presented as an open space of pore volume, then, because of these free volume effects, polymer membranes exhibit relatively high ionic conductivities. Another possible reason for a reduction of internal resistance may be caused from the presence of thinner membrane which led to a decreased pure ohmic resistance and an enhanced crossover of noble metals via the membrane under the electrochemical stress with long operation time [12]. However, in this experiment, we note that the decrease of internal resistance may possibly come from the increase of water

content inside membrane and which provide the good conductivity of exchange ion inside membrane with excess fully hydration from water and methanol solution.

Table 4.5 Cell impedance at different test times of the SCO mode.

Operating hour (hr)	Cell impedance (Ω cm^2)	
	R_s	R_{ct}
0	0.379	2.524
20	0.311	2.830
40	0.307	3.238
60	0.268	3.513
80	0.261	3.954
100	0.253	4.346

In addition, it has been reported that Nafion® was soluble in methanol solutions, and the degree of dissolution increased with the temperature and the methanol concentration [12]. Thereafter, the adsorption phenomena of intermediates changed as the Nafion® membranes lost SO_3H groups during the test period; it has been proposed that carboxylic acid end groups left over from the manufacturing process may be susceptible to attack by radical species generated during fuel cell reactions [84]. The proposed mechanism is as follows:

$$R\text{-}CF_2COOH + OH^{\bullet} \rightarrow R\text{-}CF_2^{\bullet} + CO_2 + H_2O$$
$$R\text{-}CF_2^{\bullet} + OH^{\bullet} \rightarrow R\text{-}CF_2OH \rightarrow R\text{-}COF + HF$$
$$R\text{-}COF + H_2O \rightarrow R\text{-}COOH + HF$$

The rate of SO_3H loss was faster at higher current densities and also was accompanied by the acid formation as carboxylic acid and formic acid. Under such conditions Ru dissolution was considered as significant due to the formation of acid as by-product from methanol oxidation [14, 76].

Moreover, the increased value of charge transfer resistance (Table 4.5) can imply the decrease of oxidation performance of methanol from the agglomeration of catalyst and the dissolution of Ru. Then, an activity of catalyst was reduced and it can provide the activation loss along the test of DMFC performance. The distortion of the semi-circle at higher frequencies after 60 hr to 100 hr meant that a large concentration overvoltage was generated while the cell activation loss increased [80].

4.2.2 Comparison of DMFC performance operated under different modes

The cell performance degradation of methanol-air system under SCO mode was compared with long-running operation of 100 h (LR-100). To evaluate the loss of cell performance from the loss of catalyst surface, the dissolution of Ru and the crossover of methanol were conducted. Moreover, the decaying of cell current density during test time in both SCO mode and LR-100 mode was investigated.

Figure 4.18 shows the loss of cell performance which was compared between long running operation (LR-100) and step cycling operation (SCO). The open circuit voltage (OCV) of LR-100 started at 536.6 mV and then dropped to 519.7 mV after 100 h operation. But, for the operating mode of SCO, the OCV decayed from 538.3 mV to 482.7 mV. From the comparison results, the SCO gave the higher decay rate of OCV at -0.55 mV h^{-1} which was more than the LR-100 as shown in Table 4.6. For the reduction value of cell open circuit voltage, it was dropped from the initial time at 10.3% and 2.8% for SCO and LR-100, respectively. The main drop of OCV may have come from the methanol crossover. These results revealed that LR-100 operation mode cause more catalyst surface agglomeration at anode than SCO. However, there was less methanol crossover by operating on LR-100 mode because the methanol was consumed during total 100 h test. The large crossover of methanol was occurred when the single cell was operated under SCO mode which has total 50 h to operate with no load condition. Under this no load condition, since the methanol solution was very less consumed and the high excess of methanol solution may diffuse through membrane from anode to cathode side, then, the performance of Pt-based cathode in DMFC was reduced due to the coverage with methanol adsorbate on surface of Pt. Therefore, this crossover of methanol caused the dramatic drop of cathode polarization with SCO condition.

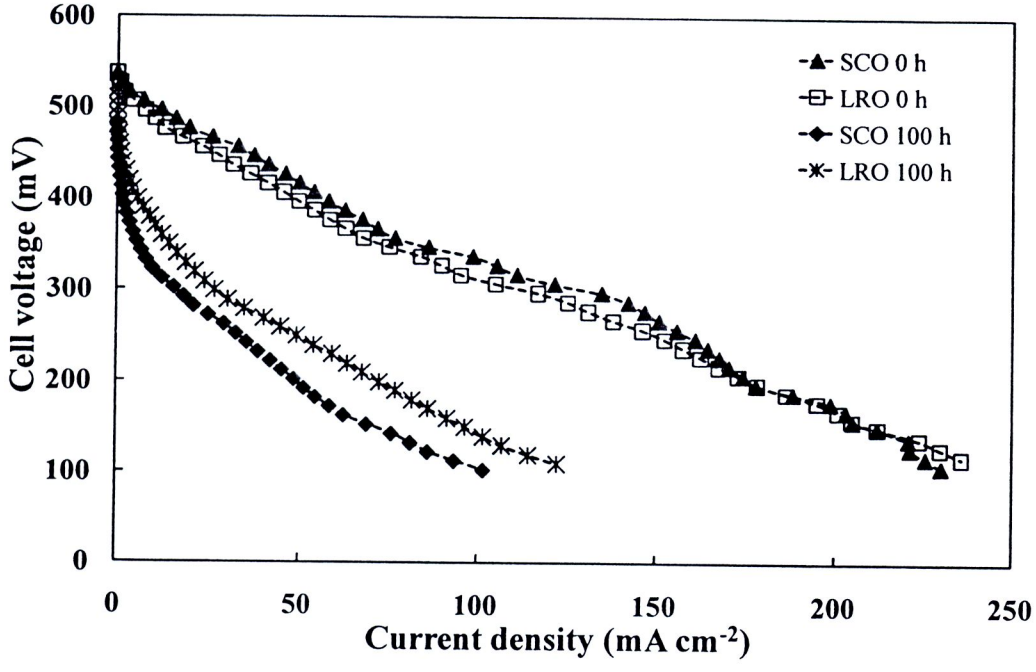

(a)

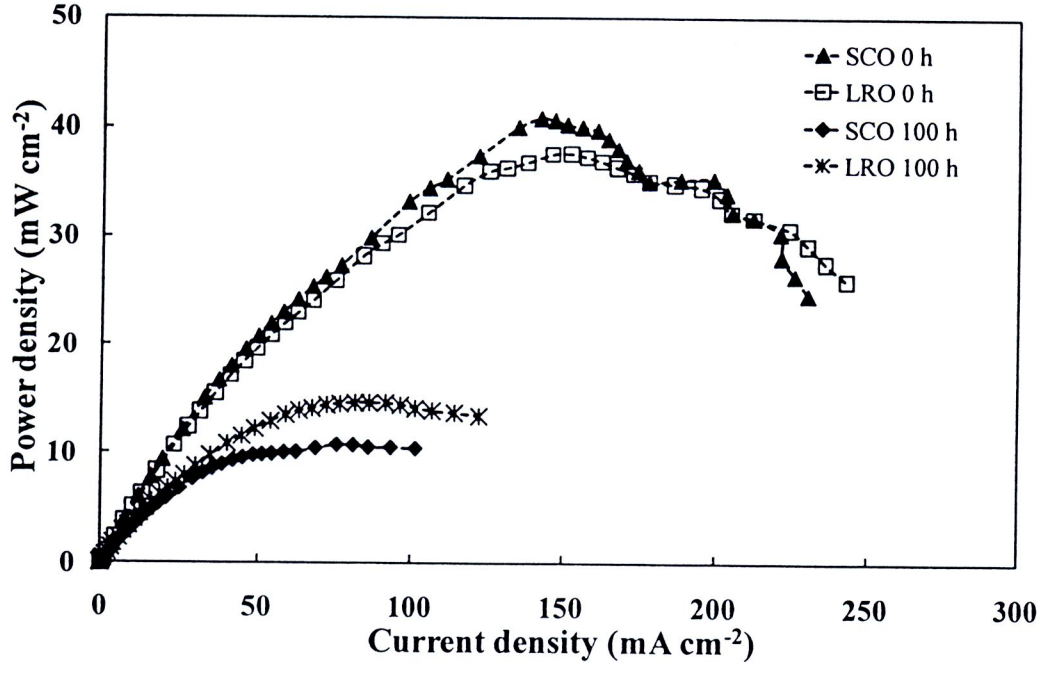

(b)

Figure 4.18 Cell performance comparison with different mode operation between LR-100 and SCO for a DMFC with 5 cm^2 active area at the initial(0 h) and the final(100 h) test time: (a) V-I curve and (b) power density curve.

For the maximum power density (Table 4.6), the loss of maximum power density was 61.1% and 73.5% for LR-100 and SCO, respectively. Also, the operating mode of SCO also provided more performance degradation with the rate of -0.30 mW cm^{-2} h^{-1} of maximum power density than the LR-100 mode at -0.22 mW cm^{-2} h^{-1}. The loss of cell power density of SCO was similar with the report of Jeon et al. [10]. So it seems that the operation mode of SCO provided the high rate of cell degradation than LR-100.

Table 4.6 Comparison of cell performance degradation rate between SCO and LR-100 modes.

Electrical value	Operating mode	Initial (0 h)	Final (100 h)	Rate of degradation
OCV (mV)	LR-100	536.6	519.7	-0.16 mV h^{-1}
	SCO	538.3	482.7	-0.55 mV h^{-1}
Maximum power ($mW\ cm^{-2}$)	LR-100	37.57	14.59	-0.22 mW cm^{-2} h^{-1}
	SCO	40.74	10.77	-0.30 mW cm^{-2} h^{-1}

The variation in current density with test time for a continuous durability test as LR-100 of the DMFC at 70 °C for 100 h is shown in Figure 4.19. The current density fell continuously with time, although the current density decline partially recovered after each intermission of measuring for cell performance degradation and renewing fuel solution. The intermission period for polarization, frequency response, and potential scan were typically for 30 minutes, after that, the current density immediately increased up nearly to the beginning value as high as possible and then continued to decay as previously. It is suggested that, there exists a short-term performance loss, which is a rapid and reversible process [12] and may be because the anode electrode surface was cleaned after applying a cyclic votammogram with the measuring technique of methanol stripping.

In addition, during the test time with constant drawing current of 100 hrs with LR-100, the cell current density at constant voltage ca., 300 mV decreased from 78.2 to 26.6 mA cm^{-2}. Comparing with SCO mode, the drop of the trend value of cell current density at different step drawing currents of load profile was increased when the current was drawn at 100 mV, 200 mV, and 300 mV, respectively. At 300 mV, the performance losses on both LR-100 and SCO were not different, but when the level of potential for drawing current

was reduced to 200 and 100 mV, the trend value more dropped further during test time at higher drawing current density values. This result trend were similar with the study of DMFC degradation by Jeon et al. [13], Guo et al. [14], and Chena et al. [61]. There was clearly a major degradation in current which implies a potentially drastic change in the cell, which is discussed in the following sections.

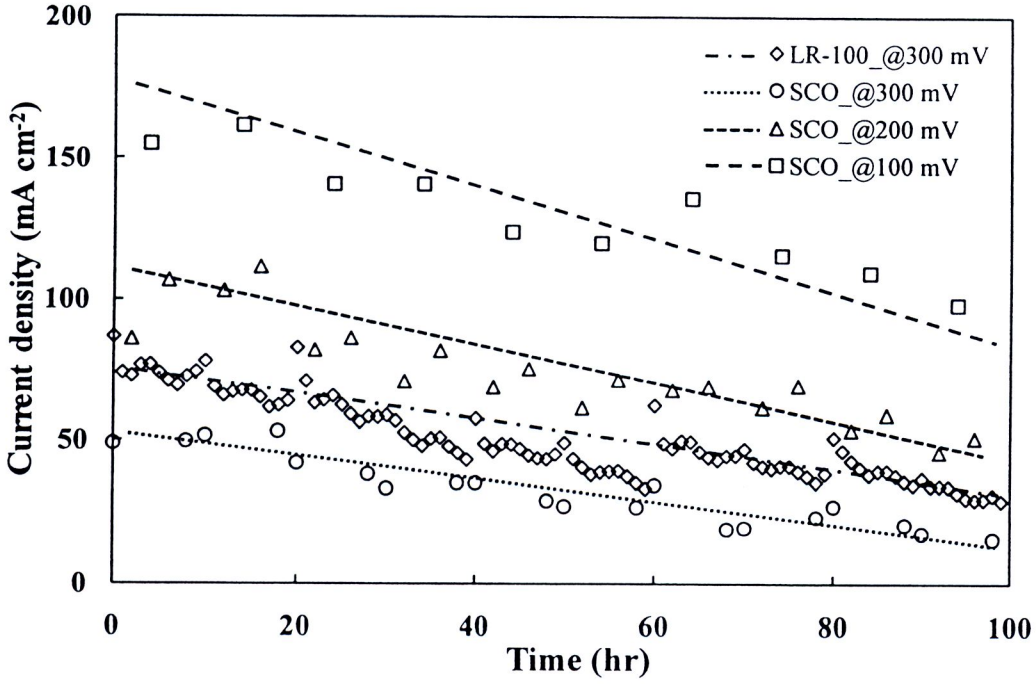

Figure 4.19 The comparison of the variation in current density with time for a DMFC with 5 cm^2 active area between operating mode of LR-100 at cell potential 300 mV and SCO at cell potential along load profile of 100, 200, and 300 mV.

For the cell parameter, the values of ohmic and activation losses were interpreted by obtaining from the slope of the cell polarization curve in terms of the area specific resistance (r) and the exchange current density (i_0) as Tafel plot, respectively, as compared in Table 4.7 and Figure 4.20. The decrease of OCV value during the test is related to the falling trend value of the exchange current density. In the same way, the maximum power density loss was increased with test time by growing area specific resistance or ohmic loss. From the data expression, the LR-100 mode gave less OCV drop than the SCO mode since the crossover of methanol caused from LR-100 was less than SCO. Moreover, the cell activation loss was represented as i_0. The high reduction of i_0 for SCO revealed the dissolution of electrode area which may from the Ru dissolution and the Ru crossover from

anode to cathode. These causes of methanol crossover and Ru dissolution served the decrease of cell performance during test time. Moreover, this cell was investigated on both anode and cathode polarization for the cell degradation behavior.

Table 4.7 The cell parameter value of open circuit voltage, exchange current density, area specific resistance, and maximum power density during test time.

Operating time	Cell parameter							
	OCV (mV)		i_0 (mA cm^{-2})		r (kΩ cm^2)		P_{max} (mW cm^{-2})	
	LR-100	SCO	LR-100	SCO	LR-100	SCO	LR-100	SCO
0	536.66	538.29	0.45	0.73	1.84E-3	1.55E-3	37.57	40.74
20	524.01	539.68	0.41	0.40	2.79E-3	3.22E-3	25.34	21.41
40	519.29	505.16	0.33	0.62	3.86E-3	4.30E-3	19.39	16.72
60	517.16	486.67	0.26	0.29	4.42E-3	6.25E-3	16.76	13.55
80	525.43	472.78	0.39	0.39	4.25E-3	5.68E-3	18.42	14.32
100	519.72	482.72	0.28	0.37	5.02E-3	7.59E-3	14.59	10.77

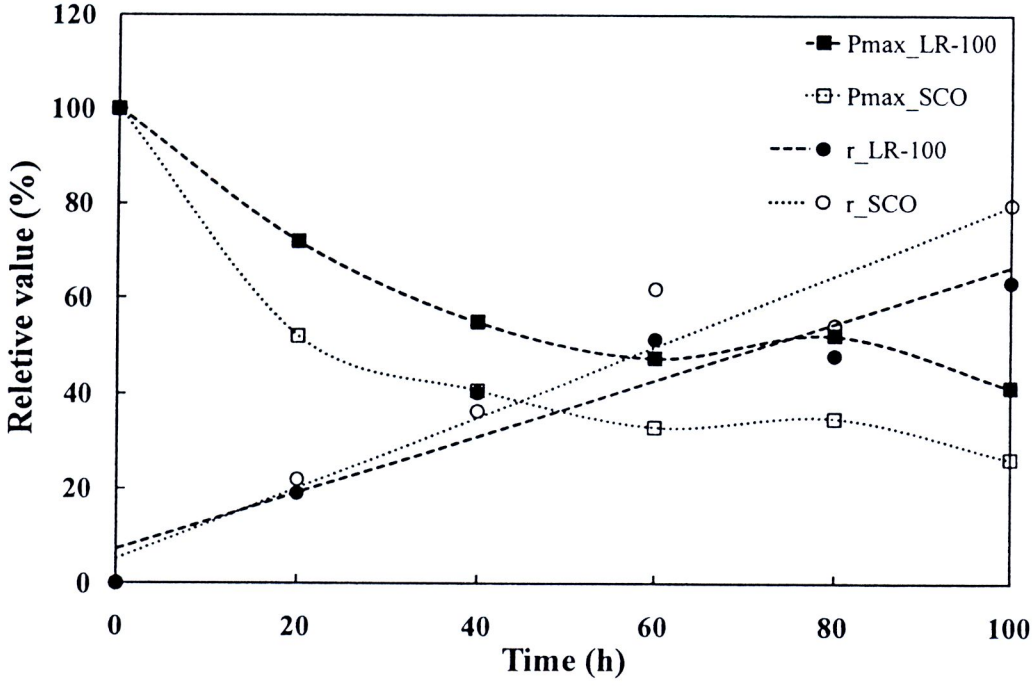

(a)

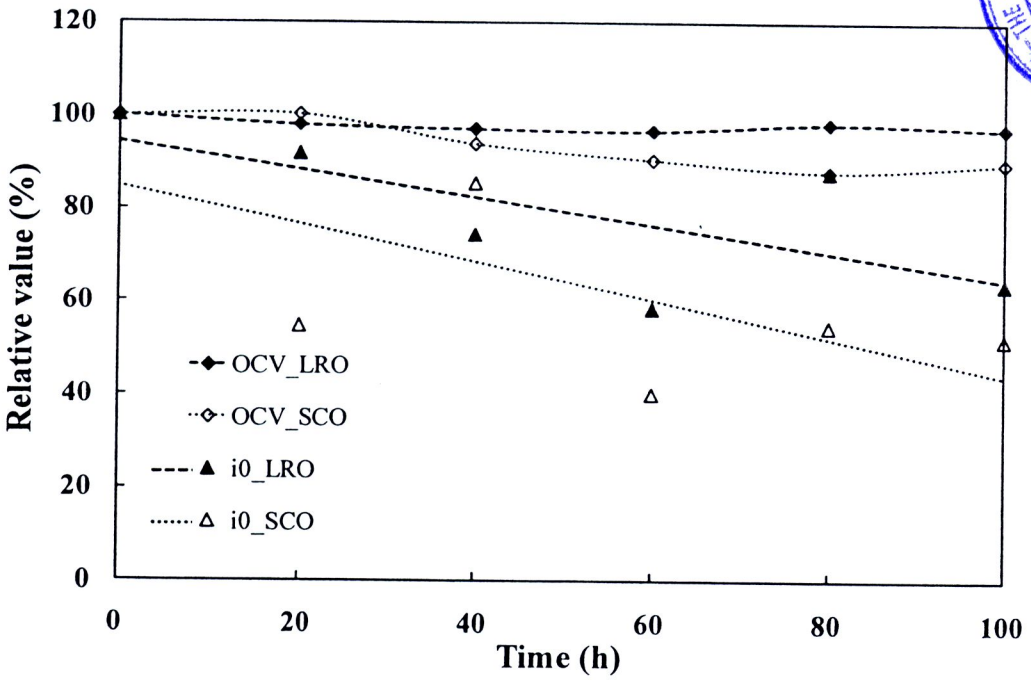

(b)

Figure 4.20 The comparison value trend of cell parameters during test time between LR-100 mode and SCO mode: (a) maximum power density and area specific resistance and (b) open circuit voltage and exchange current density.

The anode polarizations were measured at the initial (0 h) and the final (100 h) and the results were compared between LR-100 and SCO as shown in Figure 4.21 (a). By using the cathode as RHE, the anode potential was measured and used to calculate the cathode potential by subtracting from the total cell voltage. The anode polarization curves of the cell tested under the SCO mode at the beginning and 100 h operation are shown in Figure 4.21(a). The anode potential at a current density of 10 mA cm^{-2} arose from 239.9 mV (initial) to 340.1 mV (final). This increase of anode polarization might be attributed to the agglomeration of catalyst particles [75] and the loss of unalloyed Ru [15]. Furthermore, the shift of the anode potential at low current density (0-10 mA cm^{-2}) shows an instability of the catalyst surface due to the changes in electron and proton conductivity during an on-off load period in SCO mode. Besides, the anode polarization for the case of LRO mode was also plotted in Figure 4.21(a) for comparison. It must be noted that the cell working (current generating) time for the case of SCO was half of that under LRO mode although the total durability test time was the same (100 h). The increasing rate of anode

polarization in terms of potential was 1.8 and 1.2 mV h^{-1} at 100 mA cm^{-2} for SCO and LRO mode, respectively. These results revealed that SCO mode enhanced rate of anode polarization more than LRO mode.

In addition, Figure 4.21(b) shows the calculated polarization of cathode performance and the decrease of the cathode potential from the initial condition (h) to 100 h of the SCO mode was much higher than that of the LRO mode. The decreasing rates of the cathode potential (at the current density of 100 mA cm^{-2}) for the case of SCO and LRO mode were 1.8 and 0.2 mV h^{-1}, respectively. There was less methanol crossover when the cell was operated under LRO mode because methanol was continuously consumed throughout operation period of 100 h. Methanol crossover was higher when the cell was tested under SCO mode since in the SCO mode contained 50 h of no load condition. As a consequence, the performance of Pt-based cathode was reduced. Such circumstances might promote Ru dissolution and unalloyed Ru migration to the cathode side along with methanol [12, 75]. Therefore the possible causes of the cathode potential reduction were (1) the competitive reaction between methanol oxidation and oxygen reduction on the Pt surface at the cathode [82] and (2) the adsorption of RuO_x (from Ru crossover) on Pt that can reduce the surface area for oxygen reduction [79].

In this experiment, the OCV of the cell applied with SCO mode was decreased further with higher rate of fuel crossover as shown in Table 4.4 then the Ru crossover could have occurred. Also, from the previous results, we can identify that not only the metal active area loss of PtRu catalyst at anode side may be come from the main degradation parameter of particle agglomeration and Ru dissolution, but also, for this part, there was a metal as Ru crossover along with the higher rate of methanol crossover at the SCO mode compared to that of LR-100 mode.

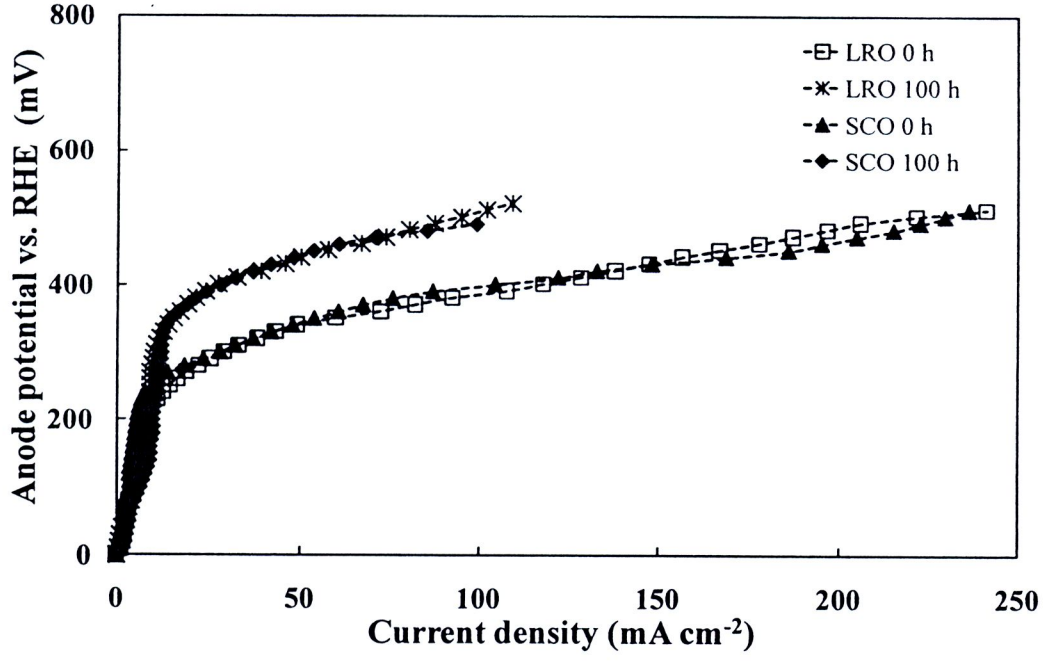

(a)

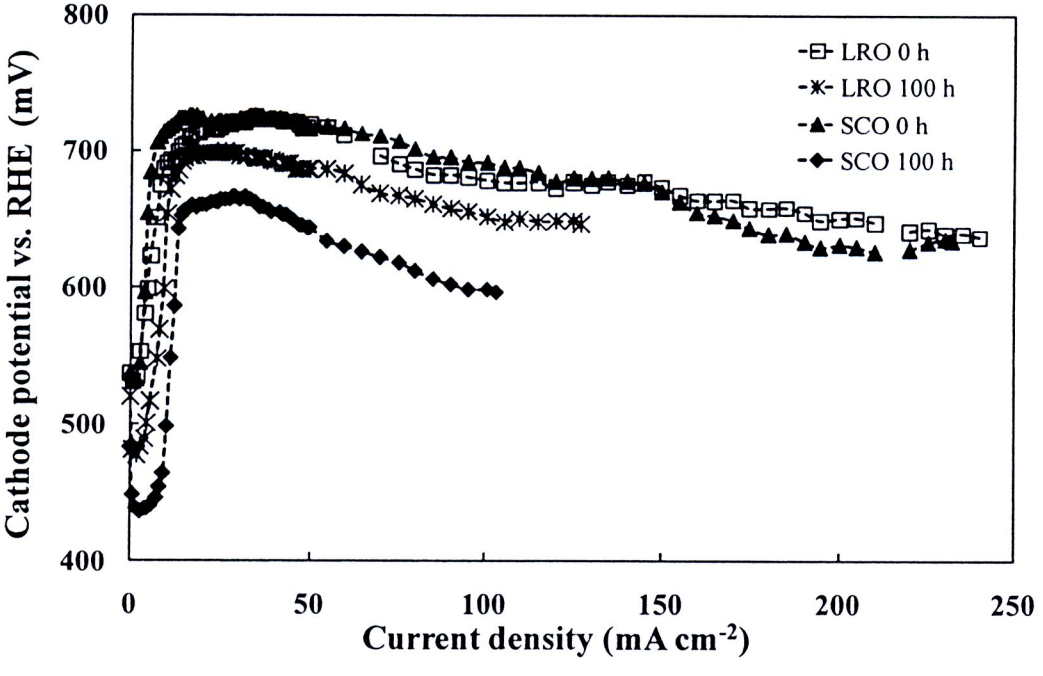

(b)

Figure 4.21 (a) Anode performance and (b) Cathode performance comparison with different test mode on LR-100 and SCO for 100 h.

To verify the cause of anode polarization especially by catalyst agglomeration and Ru dissolution, linear sweep voltammogram was performed on the anode side of DMFC. With the linear sweep voltammogram of SCO and LR-100 mode at test time of 0 and 100 h, Figure 4.22(a) shows the different oxidation current of methanol at 100 h. The same methanol oxidation current of both operation modes at initial condition (0 h) was about 60 mA cm^{-2} at around 665 mV which can represent as the based condition. After test time of 100 h, the methanol oxidation on anode electrode surface under operation of LR-100 mode gave a oxidation current lower than SCO mode, but the oxidation peak position of SCO mode was shifted to more potential than LR-100 mode respect to the based condition. These effects may come from the dissolution of Ru since the oxidation peak position of methanol or CO on catalyst surface of PtRu occurred before Pt, but, the oxidation current by PtRu catalyst was lower than Pt catalyst [87]. Another reason for the low oxidation current due to the presence of the decrement value of methanol oxidation current at 100 h was an occurring of PtRu catalyst agglomeration which can reduce the active surface area of catalyst during applying condition of LR-100.

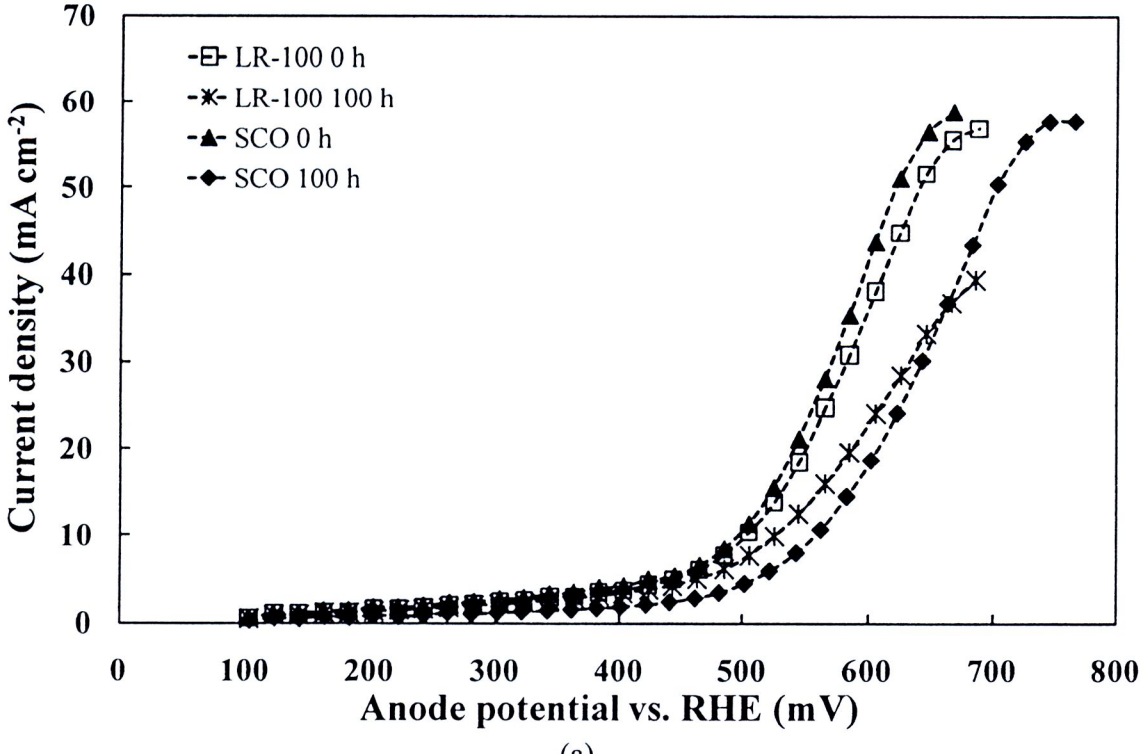

(a)

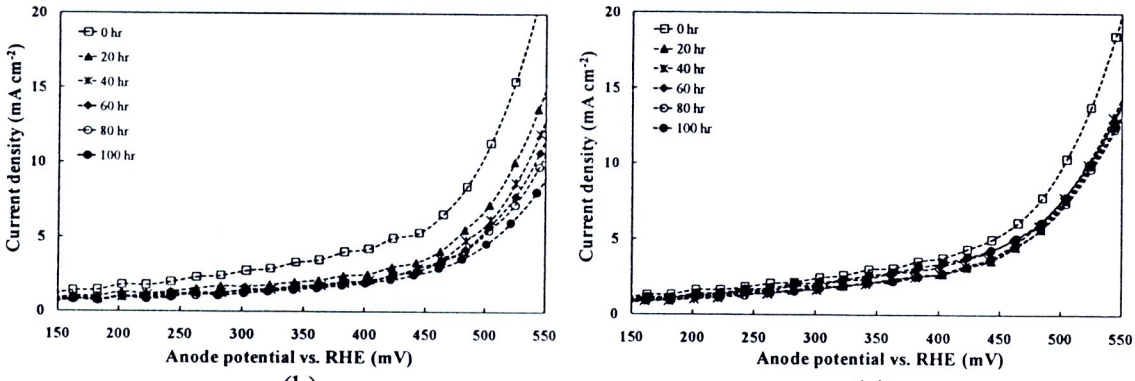

Figure 4.22 Comparison of linear sweep voltammogram of operation mode of SCO and LR-100 with temperature of 70° C (a) test time of 0 and 100 h, and also, the onset potential at different test times during 100 h operation with (b) SCO mode and (c) LR-100

Figure 4.22 shows the linear sweep voltammograms for both SCO and LRO modes, in which the onset potentials at different test times were determined and the results are summarized in Table 4.8. It shows that the onset potential at final time of the SCO mode was higher than that of the LRO mode. The increase of onset potential was attributed to the change of catalyst composition when the amount of ruthenium (Ru) was reduced [14]. Then, the influence of CO_{ads} poison on the anode catalyst was enhanced [48]. It was also reported by Láňová et al. [87] that the starting potential of CO and methanol oxidation on PtRu was lower than that on Pt.

Table 4.8 The value of anode onset potential at mode of SCO and LR-100.

Operation time (hr)	Onset potential (mV)	
	SCO	LR-100
0	239.9	275.4
20	342.0	315.9
40	363.1	335.5
60	343.4	321.3
80	363.2	322.3
100	362.8	346.8

From the linear sweep voltammogram data, the Tafel curves were plotted to determine the values of the Tafel slope and the exchange current density (i_0) at different time during 100 h of testing as shown in Figure 4.23 and Table 4.9. Normally, the Tafel slope depends on the reaction involved and the material that the electrode is made from. Its value has little impact on the activation polarization. Instead, the key parameter that outweighs the activation loss is i_0 [38]. For the SCO mode, the exchange current density during the test time decreased from 0.807 to 0.387 mA cm^{-2} in low current density region. The decrease of i_0 indicates that the performance loss of the binary PtRu catalyst may be from Ru dissolution. These results were corresponded to the increase of onset potential of methanol oxidation. Although the value of i_0 was fluctuated, it had an overall decreasing trend from its initial value for about 52.0% and 12.2% under the SCO and LRO modes, respectively. This decrease of i_0 led to the decay of cell performance curve explained by the equation of $\Delta V_{act} = Aln\left(\frac{i}{i_0}\right)$.

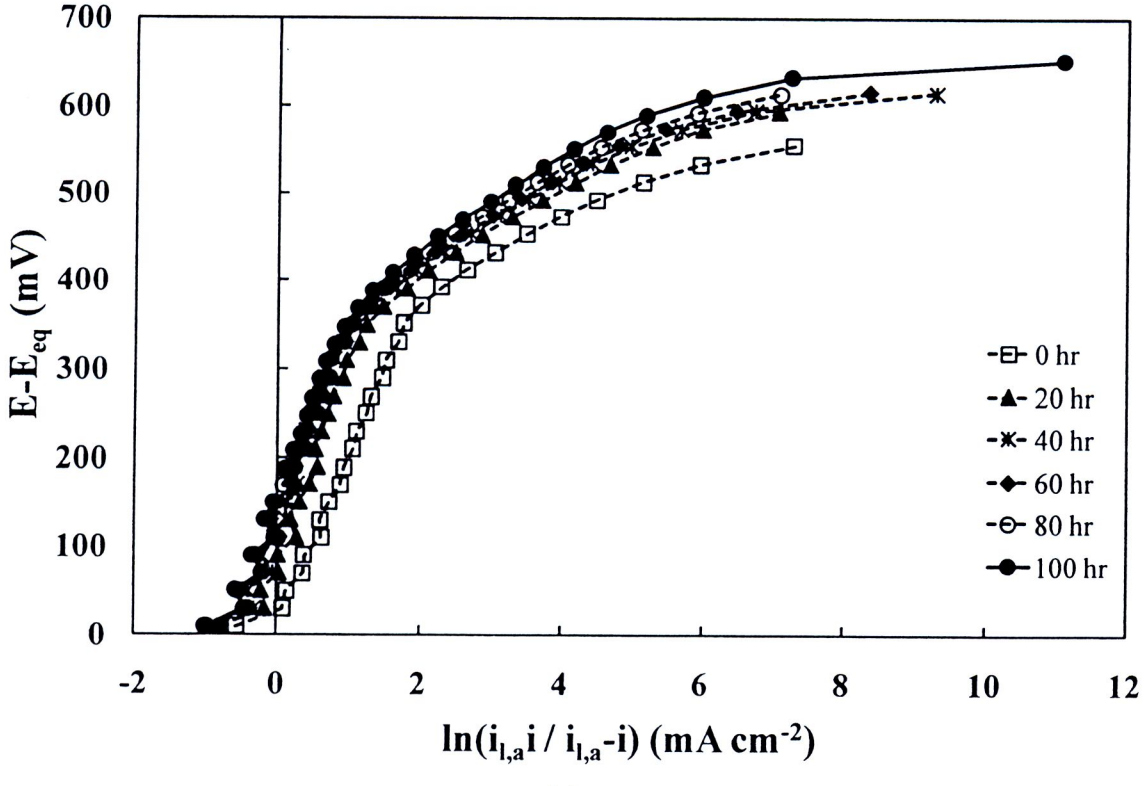

(a)

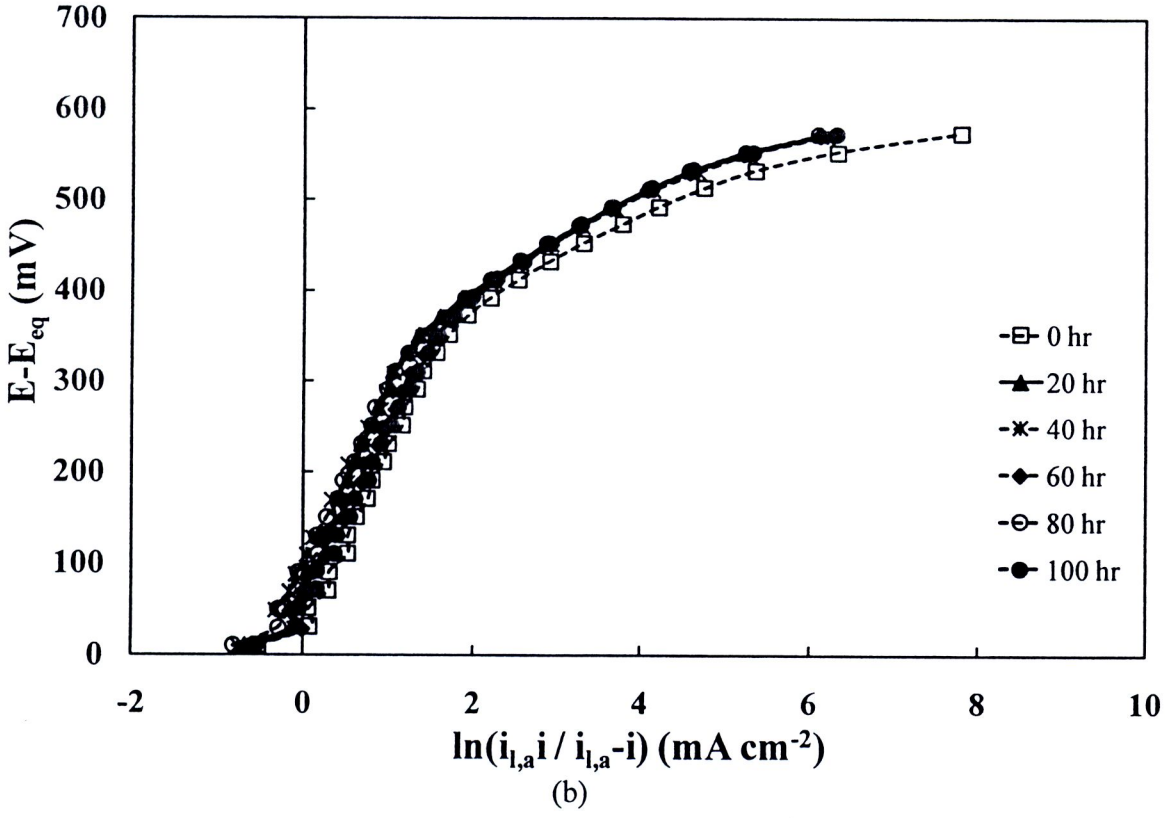

(b)

Figure 4.23 Tafel plot during test time of 100 h (a) SCO mode and (b) LR-100

Table 4.9 The value of anode Tafel slope and exchange current density (i_0).

Operation time (hr)	Tafel slope (mV dec^{-1})		i_0 (mA cm^{-2})	
	SCO	LR-100	SCO	LR-100
0	173.6	201.5	0.807	0.885
20	172.3	205.8	0.468	0.661
40	183.1	187.0	0.421	0.578
60	174.7	189.2	0.393	0.695
80	181.6	199.0	0.422	0.618
100	184.3	195.9	0.387	0.777

Characterized by FRA, anode impedances of the cell operating under the SCO mode at different test times are shown in Figure 4.24(a). The obtained Nyquist plot feature has been changed along with the test time. For the initial period (0-40 h) at low frequency,

a normal kinetic semicircle of DMFC anode impedance was observed when the trend of Nyquist curves was not distortion at the tail of the curve and was moved to positive region of Z". The Nyquist arc as semicircle shape was still until 40 h operation because, at this low frequency region, the electro-oxidation reaction of adsorbed CO and an inductive element were induced a phase delay by the slow reaction of CO_{ads}, then provide a tail of Nyquist move to the positive of Z" [12-13]. But, At 60 h of test time, the shape of semicircle at low frequency region was destroyed and moved from positive to negative region of Z" and the size of the semicircle expanded with the increase of test time reflecting the increase of charge transfer resistance, R_{ct} (from table 4.10). Under the SCO condition, this CO_{ads} oxidation phenomenon was reduced because of the loss of Ru taking place at the anode of the DMFC as time proceeded. Therefore, the distortion on the tail of Nyquist arc at low frequency was affected from the Ru dissolution.

Compared to LR-100 mode (Figure 4.24(b)), the Nyquist arc of the LRO mode extended faster than that of SCO mode but the inductive loop of the LRO mode lasted longer up to 80 h of cell operation. The faster extension of the semicircle for the case of LRO mode was the result of longer working time. For the same durability test time, the current drawing time of the anode catalyst operated under the LRO mode was twice of that under the SCO mode. From Table 4.10, the charge transfer resistance (R_{ct}) of both operation modes could be compared and found that the R_{ct} increased about 1.72 times and 1.81 times of the initial value under the SCO and LRO modes, respectively. The total increase of charge transfer resistance on both operation modes implied the decrease of anode catalyst activity in methanol oxidation.

It was also observed that the impedance spectra of the LRO mode had a higher tendency to move into the fourth quadrant, forming an inductive loop at longer time with respect to SCO mode. This phenomenon confirmed a slower dissolution rate of Ru of the cell operated under LRO mode than that under SCO mode as mentioned in all previous results. Under LRO mode, a lower concentration of methanol in catalyst layer and a lack of thermal cycle effect might slow down the Ru dissolution rate. After 80 h of operation time, however, the impedance spectra of LRO mode was similar to that of SCO mode.

At high frequencies, internal resistance (R_s) of the cells after 100 h operation under SCO and LRO modes was determined, as displayed in Table 4.10. The R_s was decreased from 0.379 Ω-cm^2 to 0.253 Ω-cm^2 after 100 h under operating condition of SCO. The reduction of R_s from the initial value was 33.2% and 13.8% for the case of SCO and LRO mode, respectively. The reduction of internal resistance was due to the increase of free volume called as "open space" in the membrane. In fact, Nafion® can absorb so much water that its volume can increase up to 22% when it is fully hydrated, however, for a strong polar liquid, like alcohol, it can cause swelling in Nafion® up to 88% [88]. This could increase the water uptake of the membrane. With high hydration in the membrane, a proton hopping mechanism became dominant leading to higher effective proton conductivity. On the other hand, the higher swelling degree of the membrane operated under SCO mode also enhanced methanol crossover leading to higher cathodic polarization.

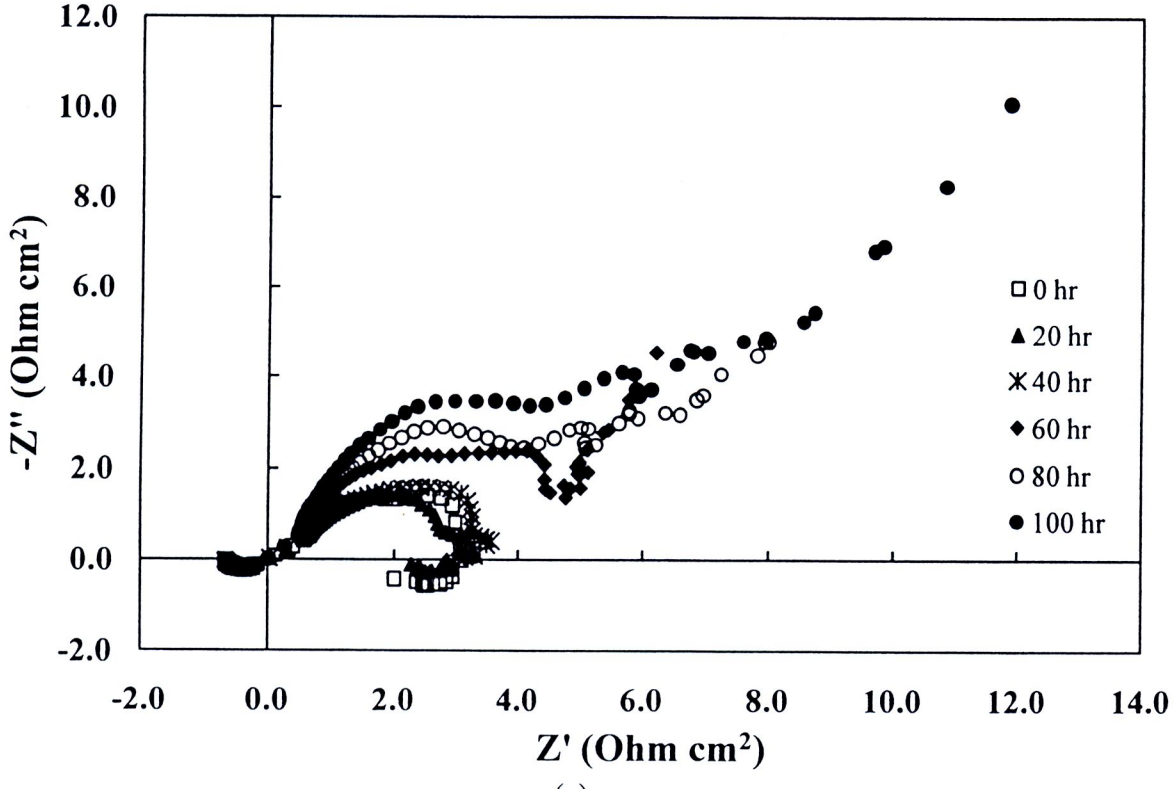

(a)

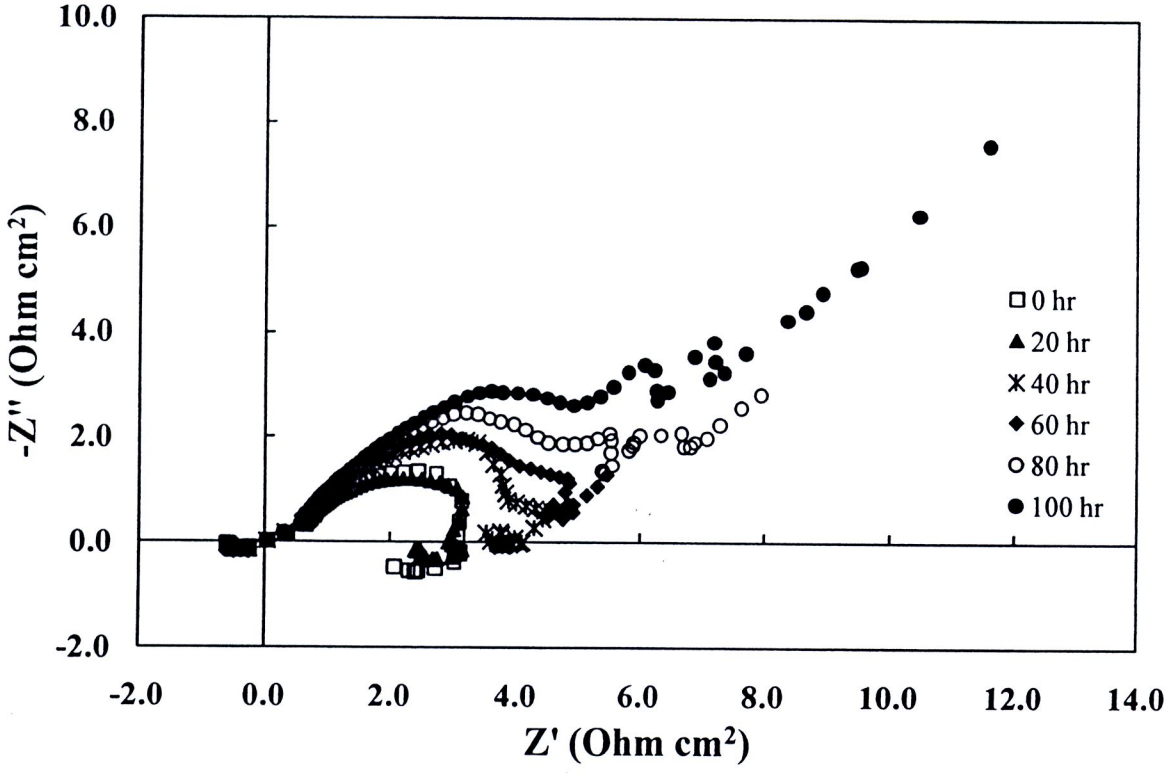

(b)

Figure 4.24 Complex plane plots of the anode impedance of PtRu/C electrode with AC amplitude 20 mV at operating DC 300 mV vs RHE under feed of 1 M CH_3OH during operating mode of (a) SCO and (b) LR-100.

Table 4.10 The value of anode internal resistance (R_s) and charge transfer resistance (R_{ct}).

Operation time (hr)	R_s (Ω-cm^2)		R_{ct} (Ω-cm^2)	
	SCO	LR-100	SCO	LR-100
0	0.379	0.354	2.524	2.934
20	0.311	0.321	2.830	3.221
40	0.307	0.322	3.238	4.454
60	0.268	0.314	3.513	3.933
80	0.261	0.316	3.954	4.612
100	0.253	0.305	4.346	5.323

4.3 Reduction of the cell performance loss

This work was extended in order to improve the cell performance with decrease of cell performance loss. In combining the advantages of both methanol and ethanol, direct alcohol fuel cells fed with mixed alcohol solutions (1M methanol and 1M ethanol in varying volume ratios) were tested for performance with employing a PtRu-PtSn/C catalyst as anode. In addition to the availability of each fuel, a favorable DAFC should be able to handle either a single alcohol or a mixed alcohol (methanol/ethanol) feed. Therefore, in this study, the DAFCs fabricated with either a mixed catalyst (PtRu-PtSn/C) or a PtRu/C catalyst were tested for their performances with methanol-and-ethanol solutions mixed in different volume ratios. The techniques of AC impedance and stripping voltammetry were used to evaluate the electrochemical activity of the catalysts and the polarization losses in the cells. Finally, the suitable catalyst for DAFC operation with mixed alcohol solutions was determined.

4.3.1 PtRu-PtSn/C cell performance with mixed alcohol fuels

The cell performance results obtained in terms of potential-current density and power density-current density curves for PtRu-PtSn/C at different ratios of mixed methanol/ethanol fuel are shown in Figure 4.25(a) and Figure 4.25(b), respectively. The highest performance was obtained when a methanol solution was the fuel, and the performance decreased with the increase of ethanol ratio in the fuel. This is not a surprising result since the electro-chemical kinetics of ethanol is much slower than that of methanol. However, the abrupt drop of power density that took place with the small addition of ethanol (2.5% by vol) in the mixed fuel was unexpected. Additionally, the cell performance was gradually reduced when the amount of ethanol in the mixed fuel was greater than 10% and finally approached that of a direct ethanol fuel cell (~15 mW/cm^2). In most published data [89,90,93-95,97], the maximum power density of a DMFC was in the range of 80-150 mW/cm^2 while the maximum power density of a DEFC was lower, with a value between 15-50 mW/cm^2. The results obtained indicate that the slow kinetics of ethanol oxidation reaction restricted the access of methanol to the active sites.

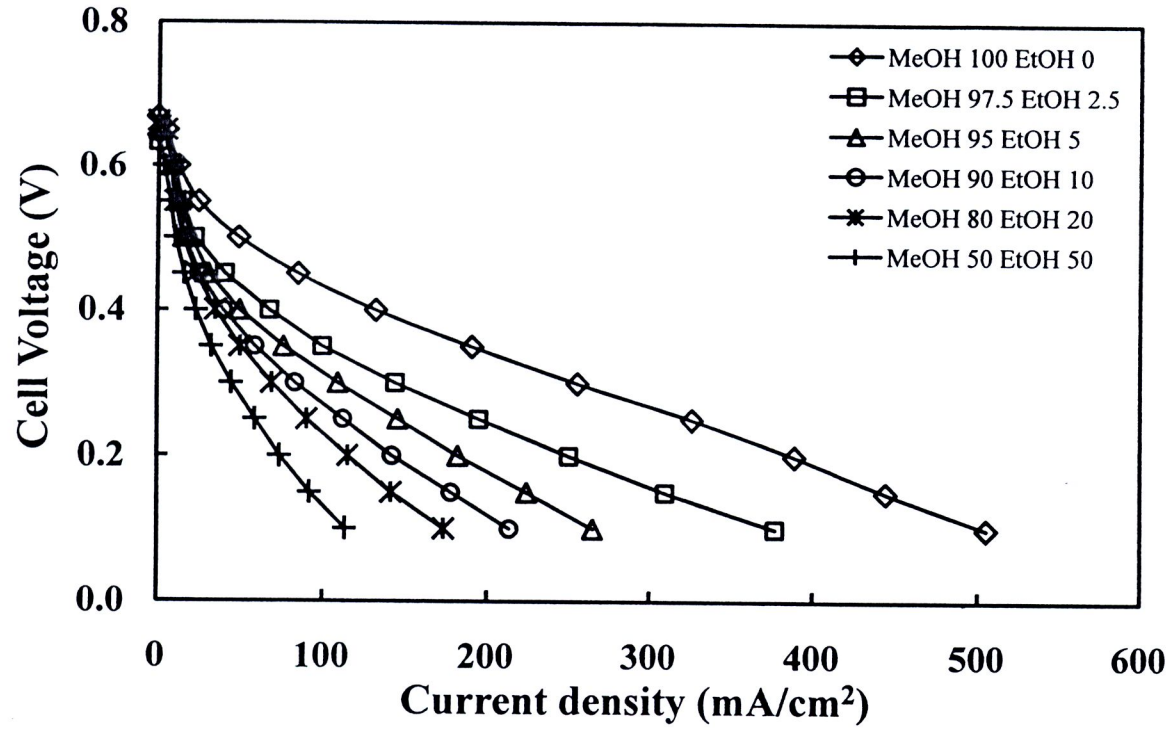

(a)

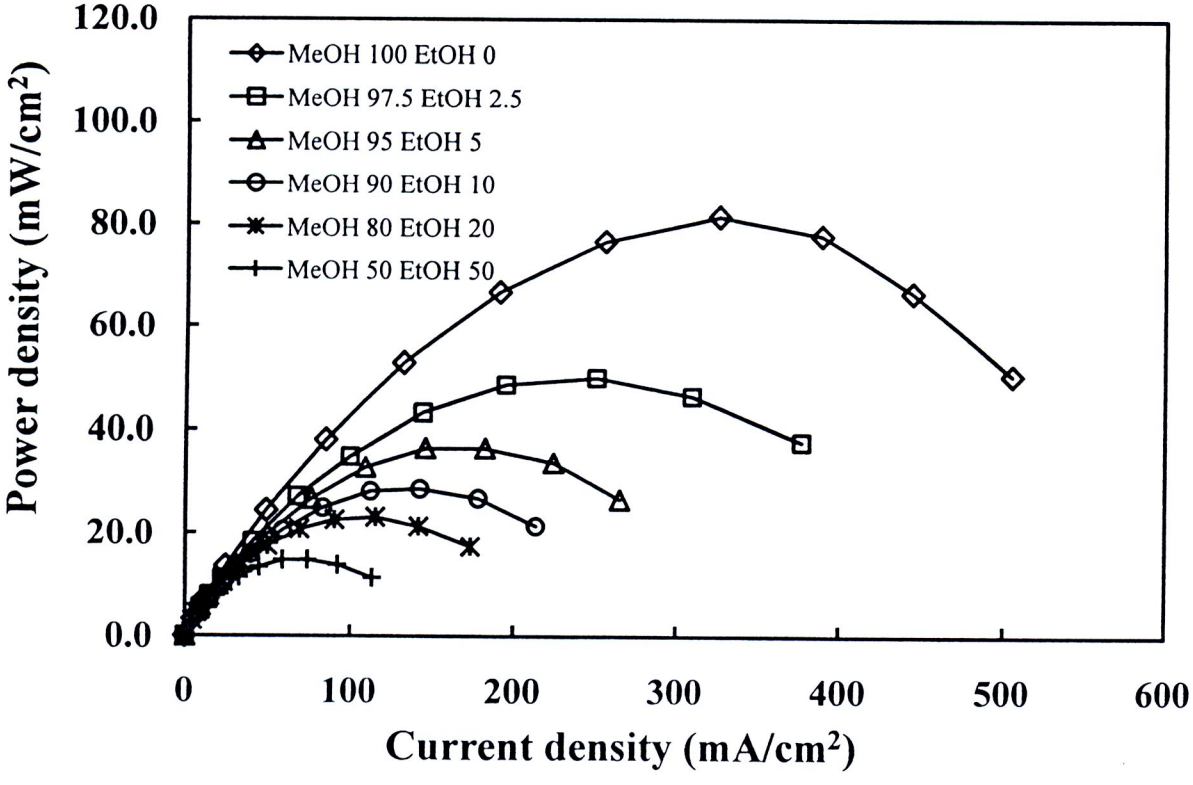

(b)

Figure 4.25 Effect of the mixed fuel ratio on PtRu/C-PtSn/C electrode performance for DAFC operation: (a) polarization curve and (b) power curve.

Figure 4.26 shows the stripping cyclic voltammogram (CV) of mixed methanol/ethanol on PtRu-PtSn/C electrode. Comparing the fuel oxidation onset potential at different volume percentages of ethanol in mixed fuel (See Figure 4.26(a)), it was found that the onset potential increased with the percentage of ethanol in the feed. The lowest onset potential at 0.225V was observed with a 1M methanol solution feed. This value is close to that of a DMFC using PtRu/C catalyst as previously reported, 0.2-0.25V vs. RHE [17]. When the percentage of ethanol was increased, the onset potential positively shifted and finally reached 0.3V, which is the value for the case of 50% by volume of ethanol. This could result from the slow kinetics of ethanol oxidation. The same order of magnitude in this value was also observed by Antolini and coworkers [90], i.e. 0.200 V and 0.275 V vs. RHE for PtSnRu/C (1:1:0.3) and PtSnRu/C (1:1:1) in 1M ethanol solution at 90°C, respectively. The higher onset potential of mixed alcohol on PtRu-PtSn/C observed in this study compared to that of ethanol solution on PtSnRu/C reported in the work of Antolini et al. might be attributed to the adsorption and dissociation of methanol on PtSn/C instead of PtRu/C. The ability of Sn to activate H_2O forming OH_{ads} and to supply the resultant OH_{ads} at low potential was lower than that of Ru, thereby deteriorating the tolerance to CO_{ads} surface poisoning of the PtRu-PtSn/C electrode.

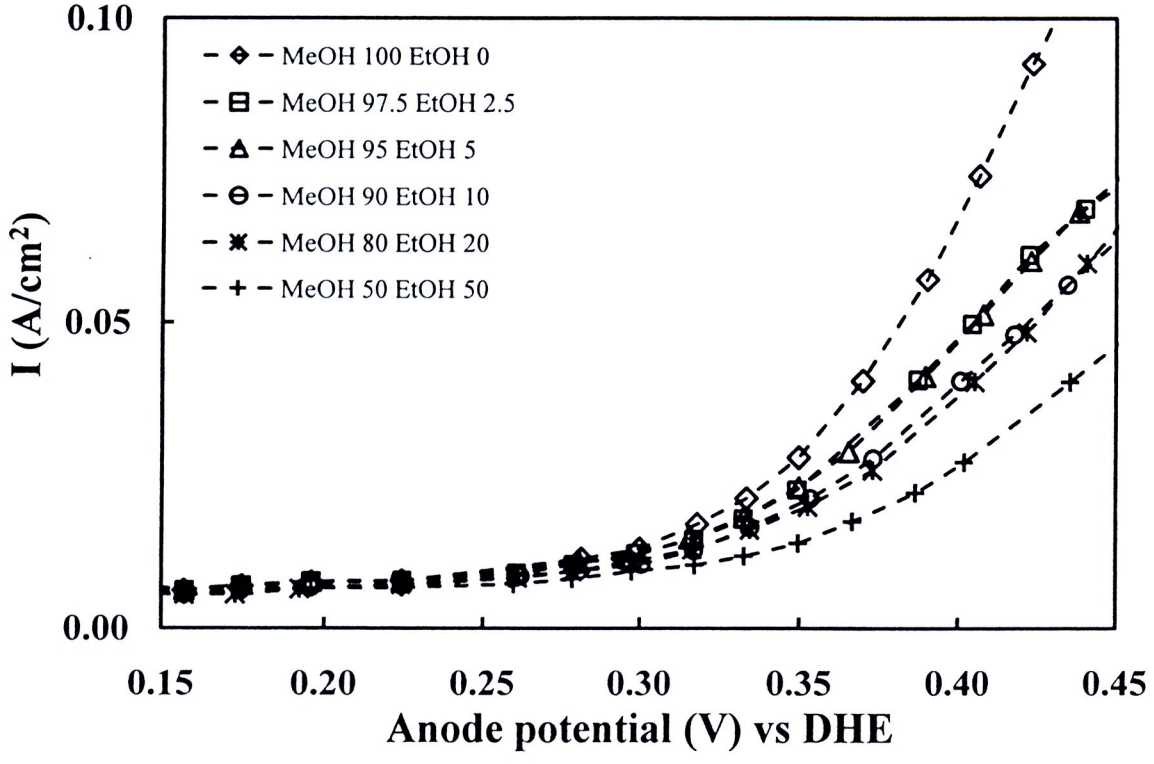

(a)

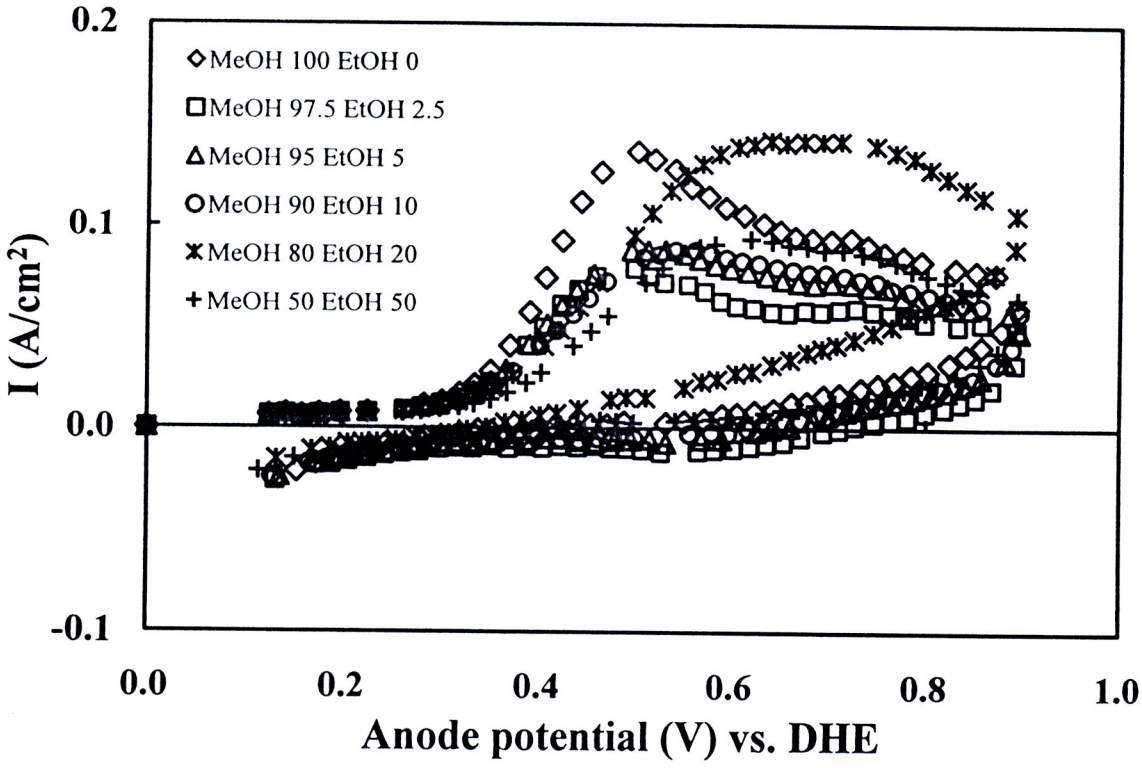

(b)

Figure 4.26 (a) Linear sweep voltammogram of the fuel oxidation onset potential and (b) Cyclic voltammogram of mixed fuel stripping on PtRu-PtSn/C electrode.

In addition, it should be noted that for the methanol stripping CV curves (See Figure 4.26(b)), two peaks appear during the forward sweep at approximately 0.5V and 0.7V, which were ascribed to the methanol and CO electrooxidation, respectively. The methanol oxidation peaks on Pt/C and PtRu/C were observed at 0.5V vs. DHE [98] and 0.55V vs. RHE [100], respectively. The CO oxidation peak on PtRu/C was depicted at 0.7 V vs. RHE by Lanova and Baltruschat [87]. For the mixed fuel stripping CV curves, the alcohol electrooxidation peak was broader and finally became a plateau when the ethanol percentage increased. This was due to a combination of methanol oxidation and ethanol oxidation on the PtRu/C and PtSn/C catalysts. Although the electrooxidation of a mixed alcohol could take place at many potential values, the current density produced by these reactions was reduced as the percentage of ethanol in the feed was increased (0.137 A/cm^2 for the methanol solution and 0.089 A/cm^2 for a 50% ethanol/50% methanol feed). The decrease in the current density was a result of ethanol engagement on the Pt active sites, and the subsequent slow oxidation reaction of ethanol became the rate-determining step.

Moreover, if the highest peak in oxidation at lowest potential occurred with the methanol solution, the declining peaks of oxidation at lowest potential for other solutions evidences that the increased ethanol reduced access to the Pt active sites of methanol.

Since the alternating current (AC) electrochemical impedance spectroscopy can provide a more precise investigation of the cause of the performance losses, the impedance spectra obtained from the PtRu-PtSn/C electrode with the mixed alcohol feed at different ratios were plotted in the form of the Nyquist plot in Figure 4.27. It was observed that the semicircle diameter increased with the increase in the percentage by volume of ethanol in the fuel. The equivalent circuit, as shown in Figure 4.28, was used to calculate the resistance of the membrane (R1), the charge transfer resistance (R2), the double layer capacity of the anode (CPE1), the electro-oxidation reaction resistance of the adsorbed CO (CO_{ads}), and the inductive element which induces a phase delay by a slow relaxation of CO_{ads} (L1) [20]. The model matches the experimental data very well ($\chi \cong 0.0028$), and the detail of fitting results are summarized in Table 4.11.

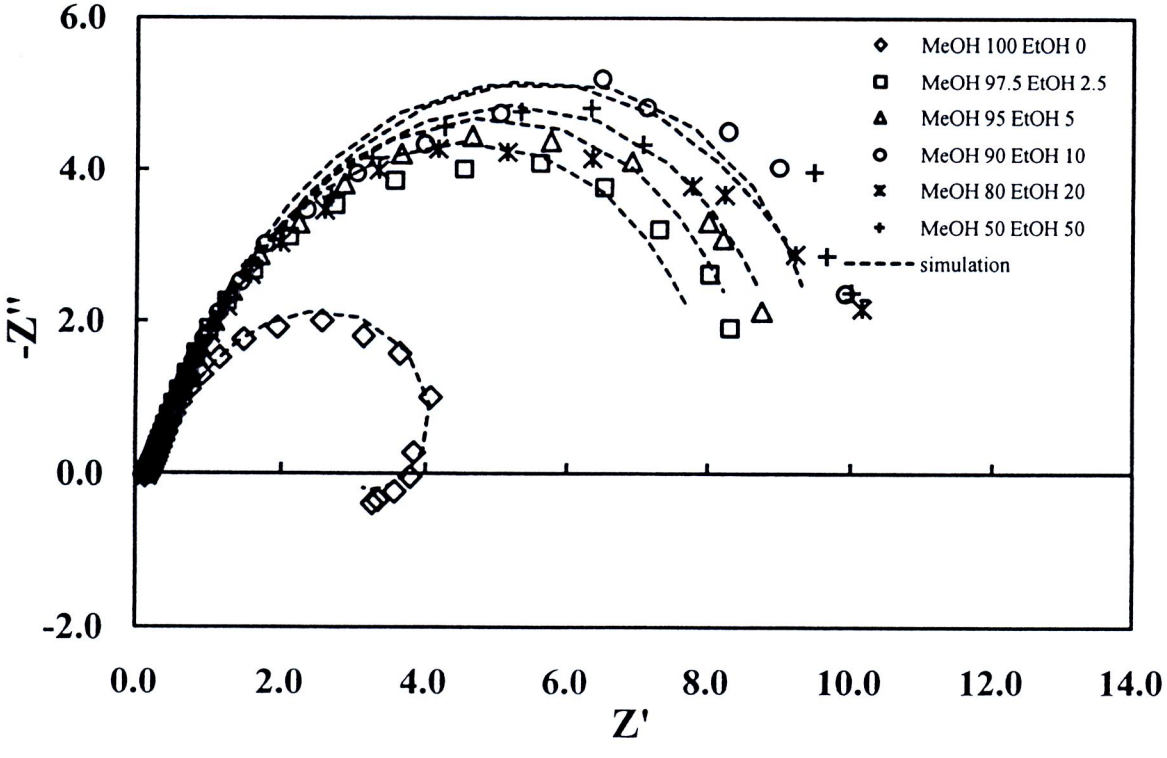

Figure 4.27 Impedance curves of the promoted Pt electrode-PtRu-PtSn-at anode fed with various mixed fuels.

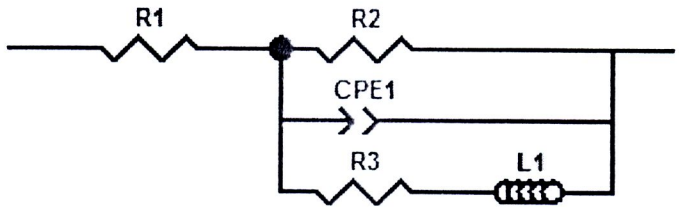

Figure 4.28 The equivalent circuit model for interpreting an impedance curve.

Table 4.11 Anode reaction resistance, charge transfer resistance and internal resistance of PtRu-PtSn/C anode operated with various mixed fuel ratios.

MeOH:EtOH (%V/V)	Circuit component resistance (Ω)			
	Anode reaction resistance	Electro-oxidation resistance of CO (R3)	Charge transfer resistance (R2)	Internal resistance (R1)
100:0	1.961	3.434	4.572	0.138
97.5:2.5	4.598	9.788	8.672	0.147
95:5	5.272	10.550	10.540	0.155
90:10	5.934	12.750	11.100	0.162
80:20	5.603	12.040	10.480	0.171
50:50	5.982	13.030	11.060	0.200

From the simulated impedance results when the percentage of ethanol in mixed fuel was increased up to 5-10%, the R2 and the R3 increased rapidly to a value approximately twice that obtained with methanol solution. Further increase of the ethanol percentage more than 10%, both R2 and R3 were almost constant. Additionally the increase of the charge transfer resistance decreased the power density of the cell as seen in Figure 4.29. The maximum power density ratio in this figure was defined as the ratio of the maximum power density obtained from each mixed fuel solution to that of a methanol solution fuel. The effect of R2 and R3 can be determined simultaneously by calculating the anode reaction resistance (ARR) which is equal to (R2×R3)/(R2+R3). Comparing the ARR of a 1M ethanol solution with that of 50/50 methanol/ethanol feed, it showed a threefold

increase from 1.961 Ω (for a 1M methanol feed) to 5.982 Ω (for a 50%/50% methanol/ethanol solution).

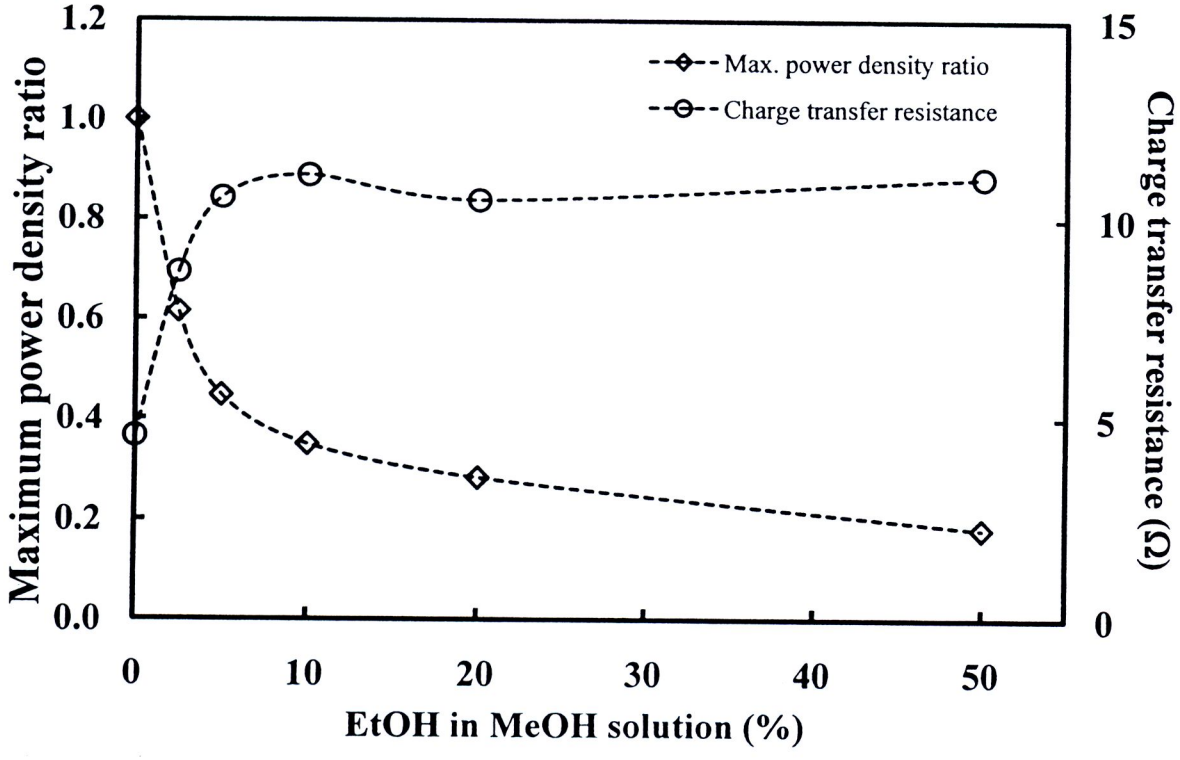

Figure 4.29 Maximum power density ratio and charge transfer resistance of PtRu-PtSn/C catalyst for the anode on the DAFC performance.

4.3.2 Performance of direct alcohol fuel cells using PtRu-PtSn/C, PtRu/C and PtSn/C catalysts fed with pure alcohol solutions

For a clear understanding of the role of the PtRu-PtSn/C catalyst in the eletrooxidation of the mixed alcohol fuels, three single cells fabricated using different electrocatalysts, PtRu/C, PtSn/C and PtRu-PtSn/C, in anode were operated with 1M methanol solution and 1M ethanol solution feed. The results of cell polarization curves and their power densities are shown in Figure 4.30. For 1M methanol solution or a DMFC operation, the PtRu/C electrode performed much better than the PtSn/C electrode, a result found by many other researchers [92-98]. For 1M ethanol solution or a DEFC operation, among these three catalysts, the PtSn/C electrode provided the highest power density, but

the difference in their performances was insignificant. The PtRu-PtSn/C electrode performance fell between that of PtRu/C and PtSn/C electrodes for both pure alcohol solution feeds. The PtRu-PtSn/C electrode performance, however, was closer to that of PtRu/C than that of PtSn/C for the case of methanol fuel, while the opposite was observed for ethanol solution feed. The reason why the PtRu-PtSn/C electrode performance for methanol electro-oxidation reaction was lower than that of the PtRu/C electrode is that the PtRu loading in the PtRu-PtSn/C electrode was half that in the PtRu/C electrode.

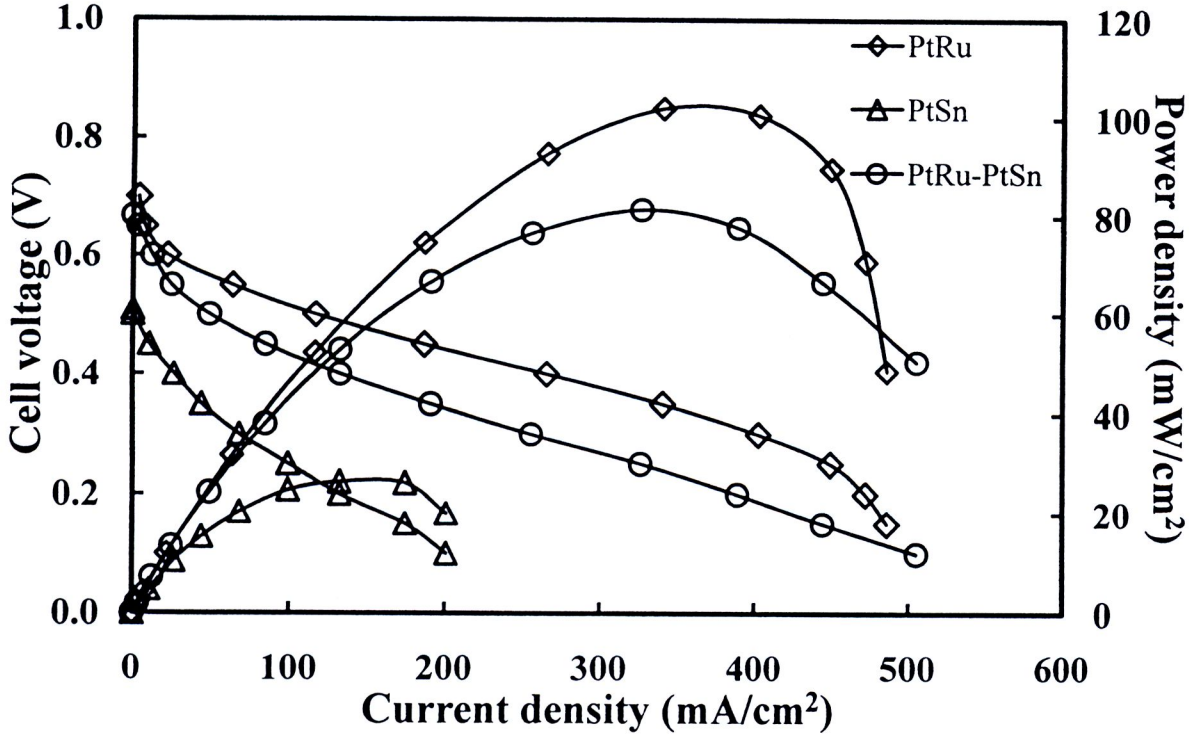

(a)

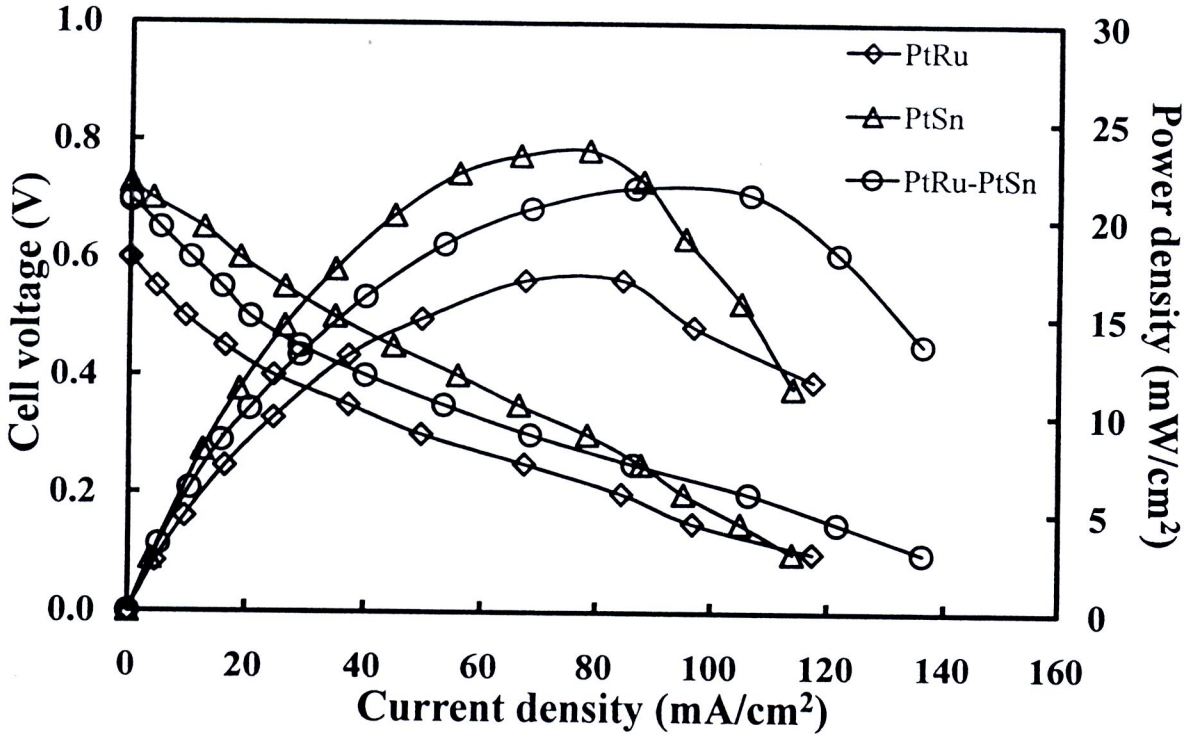

(b)

Figure 4.30 Effect of anode catalyst PtRu, PtSn, and PtRu-PtSn on DAFC performance fed with: a) 1M methanol and b) 1M ethanol.

Since the performances of PtRu/C and PtSn/C electrode in ethanol electro-oxidation were comparable, the fast drop of power density of PtRu-PtSn/C in a mixed alcohol feed (2.5% of ethanol) could be a result of the slow rate of kinetics of the ethanol oxidation on PtRu/C, rather than CO poisoning. It could be explained that, in this system, both ethanol and methanol molecules could adsorb on either PtRu or PtSn sites. If methanol molecules adsorbed on PtSn, the CO and CO-like intermediates formed during the electro-chemical reaction of methanol could poison the PtSn catalyst. Nevertheless, according to the literature [92], the methanol chemical adsorption is unfavorable on the PtSn/C due to the change of Pt electronic structure caused by PtSn alloy formation. The high performance of PtRu-PtSn/C electrode when it was exposed to the methanol solution as displayed in Figure 4.31(a) validated this explanation.

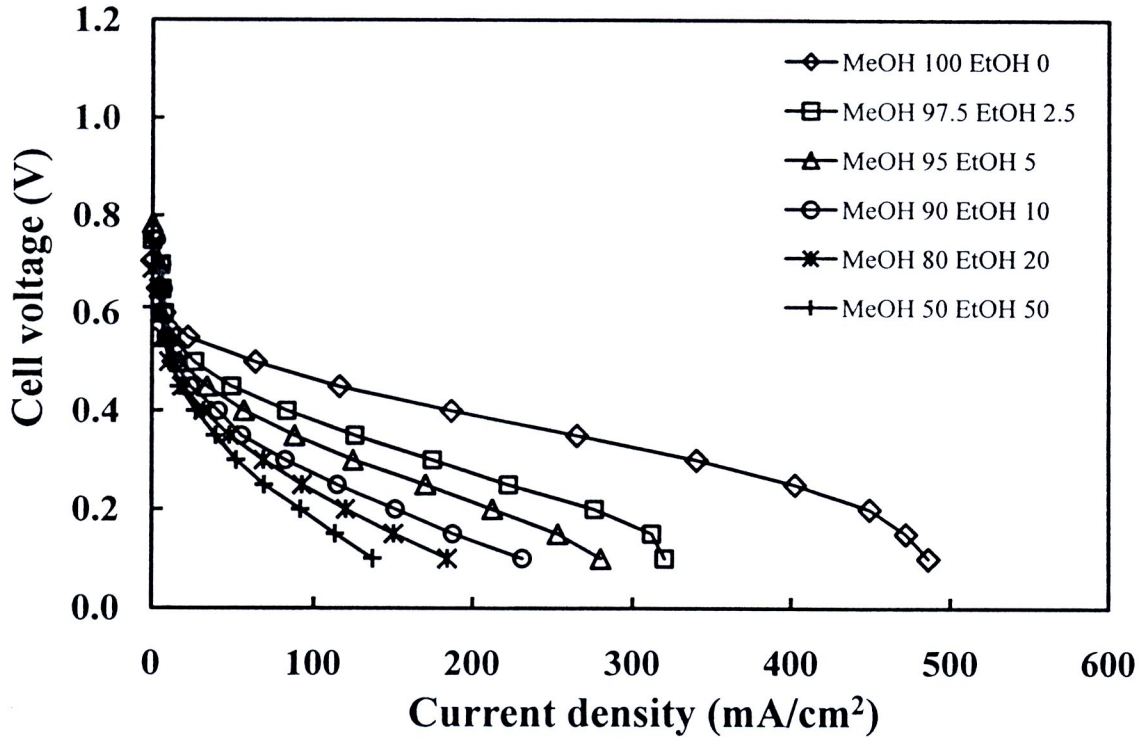

(a)

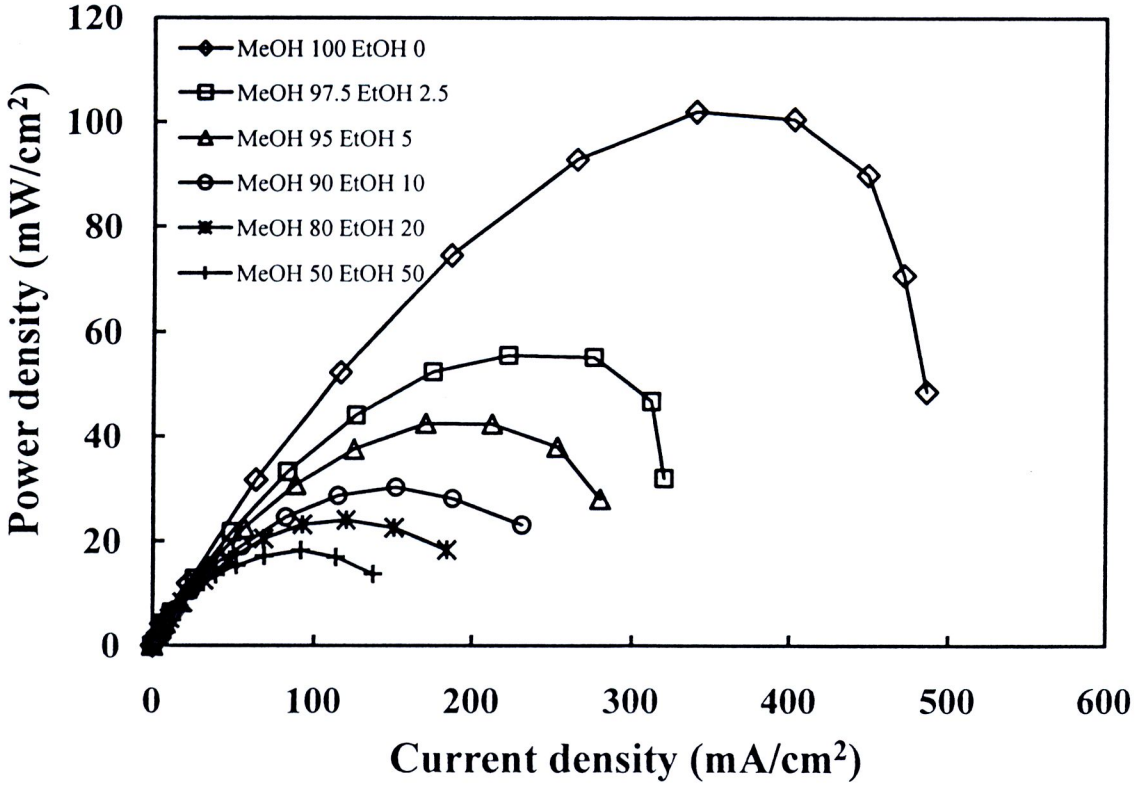

(b)

Figure 4.31 Effect of mixed alcohol ratio on PtRu/C electrode performance: (a) polarization curve and (b) power curve.

It has been known that the PtRu/C is a suitable catalyst for methanol fuel, whereas ethanol is more reactive than methanol on PtSn/C. In this work, the PtRu/C-PtSn/C showed superior performance in both feed solutions of the 1M methanol and 1M ethanol. For the methanol solution fuel, the PtRu-PtSn/C performed quite well, and it is comparable to the PtRu/C since methanol is mostly adsorbed on PtRu/C but not on PtSn/C. For the ethanol solution, although ethanol is adsorbed on either PtRu/C or PtSn/C, the PtSn/C could promote the C-C bond cleavage better than PtRu/C due to its larger lattice parameter as well as the formation of acetic acid and CO_2 as main products [92,95], which is different from the case of methanol feed. Thus, the drop of PtRu-PtSn/C performance in the mixed methanol/ethanol fuel could be caused by the undesired adsorption of ethanol on PtRu/C.

3.3 Performance of the PtRu/C cell fed with mixed alcohol solutions

In order to determine the suitable catalyst for mixed alcohol fuel, a performance test of PtRu/C with a series of mixed methanol/ethanol fuels was conducted and the polarization curves obtained are displayed in Figure 4.32. With the mixed fuels, PtRu/C electrode exhibited a similar performance drop as PtRu-PtSn/C electrode when more ethanol solution was added into the mixed fuel. Although the OCV of PtRu/C cell was higher than that of PtRu-PtSn/C cell, the voltage drop in low current density region of PtRu/C cell was greater than that of PtRu-PtSn/C cell.

For clarification, the AC impedance measurement of PtRu/C cell fed with different ratios of methanol/ethanol was also performed and all the calculated resistances are summarized in Table 4.12. It can be seen that the R1 and R2 values increased with the percentage of ethanol in the mixed fuels, whereas the R3 initially increased when the ethanol percentage increased up to 10% but decreased at higher concentration. The reduction of R3 indicated that fewer CO intermediates were formed on the Pt surface. The higher the ethanol solution ratio in the mixed fuel was, the fewer the CO intermediates were formed by electro-oxidation.

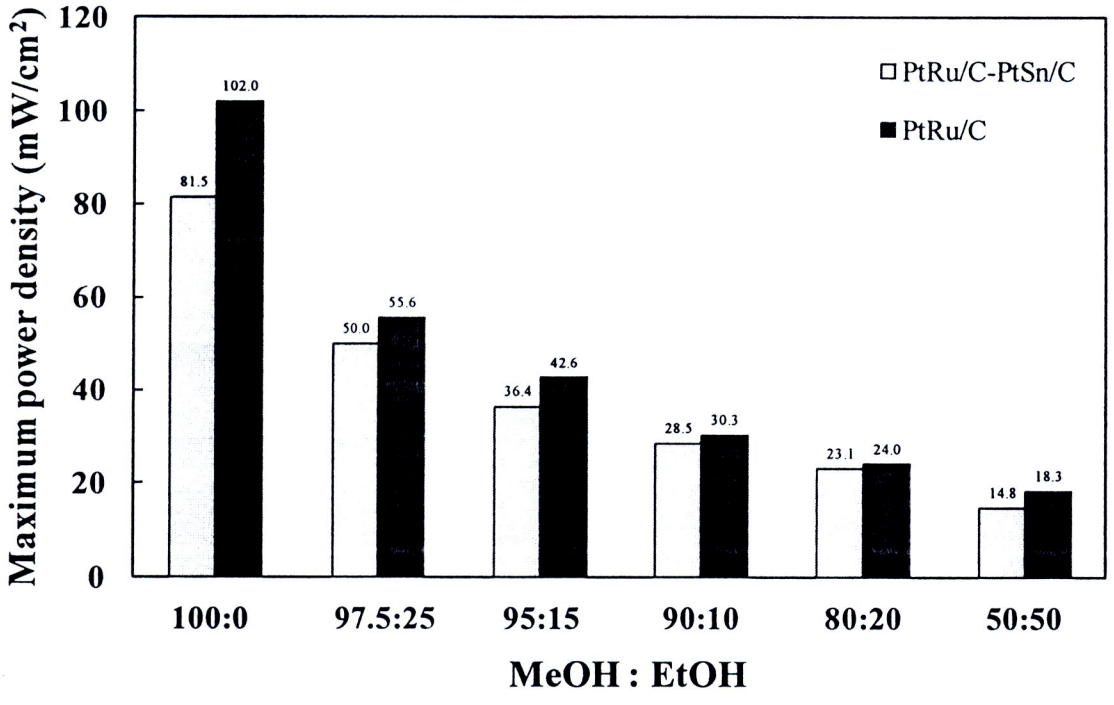

Figure 4.32 Comparison of maximum power density between PtRu-PtSn/C cell and PtRu/C cell operated with mixed alcohol solutions containing different ratios of 1M methanol/1M ethanol.

Table 4.12 Anode reaction resistance, charge transfer resistance and internal resistance of PtRu/C anode with various mixed fuel ratios.

MeOH:EtOH (%V/V)	Circuit component resistance (Ω)			
	Anode reaction resistance	Electro-oxidation resistance of CO (R3)	Charge transfer resistance (R2)	Internal resistance (R1)
97.5:2.5	11.903	29.490	19.960	0.128
95:5	16.508	52.450	24.090	0.130
90:10	21.473	75.550	30.000	0.133
80:20	19.987	56.070	31.060	0.134
50:50	20.948	38.880	45.420	0.138

In comparing the R2 and R3 resistances of the PtRu-PtSn/C and PtRu/C cells, one can notice that both values of PtRu/C were higher than those of PtRu-PtSn/C cell. The power density of PtRu/C electrode, however, was higher than that of PtRu-PtSn/C electrode. It is anticipated that AC impedance detects only the slowest kinetic rate of electro-oxidation of ethanol on PtRu/C catalyst while the faster electro-oxidation of methanol on PtRu/C takes place concurrently. The active surface of PtRu available for methanol to react for the case of PtRu/C electrode was greater than the PtRu-PtSn/C. Moreover the internal resistance of PtRu/C was lower than that of PtRu-PtSn/C because PtSn/C principally contains more oxides than PtRu/C, leading to a higher ohmic resistance of PtRu-PtSn/C catalyst [92]. Consequently, the performance of PtRu/C cell was better than that of PtRu-PtSn/C cell especially at higher current density. Figure 4.12 shows the maximum power density obtained from both PtRu-PtSn/C cell and PtRu/C cell at various ratios of mixed alcohol. From the comparison, it is clearly seen that PtRu/C was the suitable catalyst for mixed alcohol feed since it provided higher maximum power density than PtRu-PtSn/C.